Research Square

Preprints are preliminary reports that have not undergone peer review.
They should not be considered conclusive, used to inform clinical practice,
or referenced by the media as validated information.

Identification of Grem2+ Dental Follicle Stem Cells in Alveolar Bone Homeostasis and Molar Morphogenesis

Changchun Dong

dongchangchun@tongji.edu.cn

Department of Orthodontics, Stomatological Hospital and Dental School of Tongji University, Shanghai Engineering Research Center of Tooth Restoration and Regeneration, Shanghai, China

Qiongyu Zhang

Department of Orthodontics, Stomatological Hospital and Dental School of Tongji University, Shanghai Engineering Research Center of Tooth Restoration and Regeneration, Shanghai, China

Biying Yang

Department of Orthodontics, Stomatological Hospital and Dental School of Tongji University, Shanghai Engineering Research Center of Tooth Restoration and Regeneration, Shanghai, China

Jiayi Bian

Department of Orthodontics, Stomatological Hospital and Dental School of Tongji University, Shanghai Engineering Research Center of Tooth Restoration and Regeneration, Shanghai, China

Zehui Xiong

Department of Periodontology, Stomatological Hospital and Dental School of Tongji University, Shanghai Engineering Research Center of Tooth Restoration and Regeneration, Shanghai, China

Yongming Li

Department of Orthodontics, Shanghai Tongji Stomatological Hospital and Dental School, Tongji University

Article

Keywords:

Posted Date: September 1st, 2026

DOI: https://doi.org/10.21203/rs.3.rs-10692088/v1

License: This work is licensed under a Creative Commons Attribution 4.0 International License.
Read Full License

Additional Declarations: There is no conflict of interest

Abstract

Alveolar bone, derived from neural crest-derived mesenchyme, is essential for tooth support. Its regeneration remains a major clinical challenge due to its unique developmental origin and structural complexity. Dental follicle stem cells (DFSCs) contribute to alveolar bone formation, yet the specific subpopulations governing interradicular bone development and root morphogenesis remain poorly defined. Here, we identified Grem2 as a novel and specific *in vivo* marker for a distinct DFSC subpopulation. Through single-cell RNA-seq analysis and lineage tracing, we demonstrated that Grem2$^+$ cells are spatially and functionally distinct from PTHrP$^+$ and Lepr$^+$ cells, exclusively localize to the root follicle, and contribute to both cervical and basal portions of interradicular alveolar bone. Grem2$^+$ cells persist into adulthood, exhibit trilineage differentiation potential *in vitro*, and actively participate in interradicular injury repair. Conventional *Grem2* knockout in mice impaired interradicular alveolar bone formation, leading to reduced bone volume, increased bone density, and a taurodontism-like phenotype. Mechanistically, loss of Grem2 disrupted the balance between stemness and differentiation within the DFSC niche, causing premature stem cell exhaustion, accelerated differentiation, and reduced bone turnover. Together, our findings establish Grem2$^+$ DFSCs as an endogenous, periodontium-competent progenitor pool and reveal that Grem2 fine-tunes BMP and IGF2 signaling within the stem cell niche to coordinate alveolar bone homeostasis and molar morphogenesis. This study bridges a critical gap in DFSC identification, provides mechanistic insights into the pathogenesis of tooth developmental anomalies caused by *GREM2* mutations, and lays a foundation for future regenerative strategies targeting alveolar bone.

Introduction

Alveolar bone, together with the periodontal ligament, cementum, and gingiva, constitutes the periodontium, which is essential for tooth support and mastication. Unlike long bones, which derive from the mesoderm, alveolar bone originates from neural crest-derived mesenchyme and develops primarily through intramembranous ossification[1,2]. This distinct embryonic origin confers unique biological properties upon alveolar bone and its resident stem cells[2]. Critically, the formation and maintenance of alveolar bone are intimately dependent on the presence of teeth, arising from complex interactions between dental epithelium and ectomesenchyme and proceeding in coordination with tooth root development[1,3]. Clinically, alveolar bone defects caused by tooth extraction, periodontal disease, jaw cysts, trauma, or tumor resection are highly prevalent, often leading to tooth loosening or loss and severely compromising quality of life. However, alveolar bone regeneration remains a major clinical challenge due to its intricate structure and unique developmental program, underscoring the imperative to elucidate its developmental origin, cellular composition, and homeostatic regulation[4,5].

Alveolar bone is derived from dental follicle stem cells (DFSCs), which share common properties with other dental mesenchymal stem cells (MSCs)[6]. Recent advances in genetic lineage tracing and single-cell RNA sequencing have revealed remarkable heterogeneity among dental MSCs, uncovering a growing

diversity of mesenchymal cell subpopulations in vivo[3,6–8]. Markers such as Prx1, Gli1, PTHrP, Lepr, Pax9, α-SMA, and Axin2 have been employed to label DFSCs or periodontal ligament stem cells (PDLSCs) during early tooth development or adult homeostasis[3,6–11]. Nevertheless, the broad expression patterns of Prx1, Gli1, Pax9, and Axin2 in both dental pulp and periodontal tissues preclude their utility in discriminating DFSCs from dental pulp stem cells (DPSCs)[8,11]. Previously characterized markers, such as PTHrP and Lepr, label cells that differentiate predominantly into the periodontal ligament and alveolar cryptal bone, with little or no contribution to the crown or dentin–pulp complex[3,7,12,13]. Notably, PTHrP$^+$ cells preferentially contribute to osteoblasts and osteocytes in the cervical portion of the cryptal bone (i.e., interradicular and interseptal bone), while their contribution to the basal bone is substantially diminished [5,7]. Similarly, Lepr$^+$ cells, extensively studied in alveolar bone and periodontal ligament homeostasis[3,12,13], are only sparsely distributed within alveolar bone and are likewise restricted to the cervical portion of the interradicular bone[6]. The limited and spatially confined contributions of both PTHrP$^+$ and Lepr$^+$ cells to the interradicular region raise the possibility that an alternative cellular source supplies the bulk of interradicular alveolar bone, particularly its basal portion. Collectively, these observations indicate that additional DFSC subpopulations exist beyond those demarcated by PTHrP or Lepr, highlighting the need for more specific DFSC markers to comprehensively delineate the properties of these cells.

Spontaneous mutations provide an unbiased avenue for discovering key genes essential for craniofacial development[14]. Identifying and understanding such genes is critical for elucidating the genetic etiology of craniofacial abnormalities. Gremlin-2 (Grem2), a member of the DAN family of BMP antagonists that primarily binds to and inhibits BMP2 and BMP4 activity, has emerged as a critical modulator in tooth development[15–18]. Human *GREM2* mutations are associated with a spectrum of dental anomalies, including tooth agenesis, microdontia, taurodontism, and short roots, whereas *Grem2*-deficient mice exhibit shortened incisors[15–18]. Despite this compelling genetic evidence, the specific molar phenotypes resulting from Grem2 deficiency in mouse models remain poorly characterized. Furthermore, current understanding of Grem2 is largely confined to its role as a BMP antagonist; the cellular sources of Grem2 secretion and the mechanisms by which Grem2 orchestrates the tooth developmental milieu have yet to be elucidated.

Emerging evidence indicates that BMP antagonists fulfill functions beyond simple signal inhibition; they also play critical roles in establishing stem cell niches and maintaining tissue homeostasis[19–21]. The BMP family provide some of the most critical signals to suppress cell proliferation and promote differentiation and migration, while the BMP antagonists, together with BMP ligands, they create signaling gradients that govern stem cell maintenance and differentiation[19]. For example, in the intestine, trophocytes adjacent to intestinal stem cells (ISCs) at the crypt base express another BMP inhibitor Grem1, thereby creating a localized low-BMP microenvironment that sustains ISC maintenance and self-renewal[22,23]. Also, Grem1-expressing cells define a population of osteochondroreticular stem cells in the bone marrow, as well as reticular stem cells in the small intestine and a progenitor population

in the skin[24]. Such findings underscore the potential of BMP antagonists to serve as stem cell markers and niche determinants across diverse tissues.

Therefore, we hypothesized that Grem2 is secreted by stem cells or niche cells, and that *Grem2* mutation or knockout disrupts the balance between stemness and differentiation, ultimately leading to dental developmental anomalies. To test this hypothesis, we performed reanalysis of single-cell RNA-seq data combined with lineage tracing to investigate the identity and progeny of Grem2$^+$ cells. We identified Grem2 as a novel in vivo marker for a distinct subset of DFSCs. Notably, Grem2$^+$ cells persist into adulthood and contribute to interradicular injury repair. Using a conventional *Grem2* knockout mouse model, we explored the mechanisms by which Grem2 mutation leads to dental developmental anomalies. Genetic ablation of Grem2$^+$ cells resulted in tooth root dysmorphology, whereas conventional knockout of *Grem2* impaired interradicular alveolar bone formation, giving rise to a taurodontism-like phenotype. Mechanistically, Grem2$^+$ DFSCs secrete IGF2 to fine-tune local signaling and regulate root morphology. Collectively, our work identifies an endogenous, periodontium-competent progenitor pool and reveals how Grem2 integrates stem cell niche regulation with alveolar bone homeostasis and molar morphogenesis, thereby offering novel targets for biological root substitutes and periodontal regeneration.

Results

Grem2 marks a distinct dental follicle subpopulation during tooth root development

Several recent studies have leveraged single-cell resolution approaches to investigate the development of craniofacial and tooth development[5–7,25]. In the present study, we first analyzed single-cell RNA sequencing (scRNA-seq) data from mouse molar development (GSE189381), which encompasses key developmental stages including the bud-to-bell stages (E13.5, E14.5, E16.5) and the crown-root transition stages (P3.5, P7.5) (Fig. 1A). Unsupervised clustering was initially performed, and cell types were annotated using SingleR to distinguish epithelial, mesenchymal, immune, perivascular, and neuronal populations (Fig. 1A, a–e). As expected, the mesenchymal compartment exhibited considerable heterogeneity. To further resolve cellular identities within the dataset, we applied a previously established dental cell type atlas and the subpopulation markers in the original research to perform the annotation[25]. Consistent with prior reports[6], the mesenchyme segregated into dental follicle and dental papilla populations as early as E14.5(Fig. 1A, b), and subsequently gave rise to lateral follicle, apical follicle, coronal papilla, and apical papilla domains by the bell stage (E16.5)(Fig. 1A, c). Notably, the dental follicle domains were already established at E14.5, and segregated into apical follicle and lateral follicle subpopulations. The cellular organization at P3.5 and P7.5 resembled that at E16.5 but exhibited greater separation among clusters along the UMAP, reflecting ongoing differentiation processes.[6] Importantly, the lateral follicle population displayed greater transcriptional distance from other mesenchymal clusters on the UMAP projection as early as P3.5(Fig. 1A,d), and remained distinctly

separated from other groups at P7.5(Fig. 1A, e). This persistent transcriptional segregation suggests a unique and specialized function of the lateral follicle population during the crown–root transition in molars.

Next we explored the expression of Grem2 during molar development, we characterized its transcript levels from E13.5 to P7.5 (Fig. 1A, f-j). We found that Grem2 was broadly expressed in the dental mesenchyme at early stages, became enriched in the dental follicle beginning at E16.5 (Fig. 1A, h), and was uniquely expressed in the lateral follicle population during postnatal stages, suggesting that Grem2 may serve as a marker for the lateral follicle. We next evaluated two well-established dental follicle stem cell markers, Gli1 and Pthlh (encoding PTHrP)[7,11,26] (Fig. 1A, k-t). As expected, Gli1 was widely expressed across nearly all populations examined, including mesenchymal cells, epithelial cells, neurons, perivascular cells, and immune cells throughout molar development, consistent with previous researches[26,27]. This broad expression pattern indicates that Gli1 does not function as a specific marker for postnatal dental stem cells but rather reflects the general activation of Hedgehog signaling in these cells[8]. In contrast, Pthlh expression became restricted to dental follicle populations after E16.5; however, it marked both the apical follicle and the lateral follicle—two distinct populations[6]. Taken together, these findings suggest that Grem2$^+$ cells may represent a unique subpopulation within the Gli1$^+$ or Pthlh$^+$ lineages. In terms of specificity, Grem2 may offer an advantage over Gli1 and Pthlh as a marker for the lateral follicle subpopulation.

To better understand the cellular heterogeneity and functional role of the dental mesenchyme during mouse molar root development, we subclustered mesenchymal cells from molars at P3.5, a stage when root development is about to initiate (Fig. 1B,C). Subpopulations were annotated according to previously established criteria[6]. *Grem2* was predominantly expressed in a subpopulation of the lateral follicle, with a smaller proportion detected in the apical follicle (Fig. 1C). the expression pattern of *Grem2* was validated within the lateral follicle by in situ hybridization at P3.5 (Fig. 1D). Notably, *Grem2* expression became restricted to the follicle region beneath the future enamel dentin junction. The specificity and robustness of Grem2 expression in the dental follicle subset suggest its functional contribution to unique regulations in the region. To distinguish with previous lateral follicle annotation[6], we designate this subpopulation as the root follicle.

We next explored the relationship between Grem2$^+$ cells and previously characterized dental follicle progenitor populations, including Gli1$^+$, Pthlh$^+$, Prrx1$^+$, Acta2$^+$, Cxcl12$^+$, and Lepr$^+$ cells[3,7,8,10,11,26]. Grem2$^+$ cells represent a distinct subpopulation that exhibits partial overlap with other dental follicle progenitor clusters. Reflecting the greater specificity of Grem2$^+$ cells, the proportion of Grem2 expression within other dental follicle progenitor populations ranged from 3.17% to 8.06%. In contrast, the proportion of other dental follicle progenitor markers expressed within Grem2$^+$ cells ranged from 29.03% to 76.03% (Fig. 1E). Among these markers, Grem2$^+$ cells showed the highest correlation with Acta2$^+$ cells (Fig. 1F), which have been reported to label periodontal ligament (PDL) cells in mouse incisors[28]. These results indicate that Grem2$^+$ cells represent a highly specific subpopulation within the dental follicle lineage, and

Grem2⁺ cells may serve as a dedicated precursor pool for the periodontium, particularly the alveolar bone and periodontal ligament compartments, during root development.

We next compared the differential gene expression (DEG) profiles of Grem2⁺ and Grem2⁻ cells. *Igfbp3*, *Id2*, and *H19* were highly expressed in Grem2⁺ cells (Fig. 1G). Id2 has been shown to maintain the precursor cell state of mesenchymal stem cells (MSCs), preventing premature differentiation[29], while Igfbp3 has been implicated in stem cell regulation[30]. Gene Ontology (GO) analysis revealed enrichment of terms related to ossification, epithelial cell proliferation, and osteoblast differentiation in Grem2⁺ cells (Fig. 1H). Together, these findings indicate that Grem2⁺ mesenchymal stem cells constitute a unique progenitor population in a primed activation state, exhibiting pronounced osteogenic lineage commitment and an active role in modulating tooth germ morphogenesis.

Grem2⁺ Cells Represent a Distinct Progenitor Population of the Dental Follicle

The dental follicle, a key ectomesenchymal tissue, comprises a heterogeneous cell population. To date, two main strategies have been employed to isolate dental follicle stem cells: microdissection based on anatomical location, or targeted isolation using known in vivo molecular markers via techniques such as fluorescence-activated cell sorting (FACS)[31,32]. The previously published scRNA-seq dataset (GSE189381) was generated using the microdissection approach and encompassed all cell types within the tooth and surrounding tissues[6]. In this dataset, the dental follicle cell subpopulation constituted only a small fraction of total cells, potentially introducing biases related to sequencing depth. Moreover, this method lacked an intrinsic lineage label, limiting the ability to definitively track specific subpopulations. To further elucidate the role of Grem2⁺ cells within the dental follicle and clarify their relationship with established *in vivo* markers, we analyzed scRNA-seq datasets derived from FACS-sorted Gli1⁺ (GSE237439) or PTHrP⁺ cells (GSE313714 and GSE120108) to determine the distribution and functional characteristics of Grem2⁺ cells[5,33].

We first examined the distribution of Grem2⁺ cells within the Gli1⁺ cell population using a published scRNA-seq dataset (GSE237439) [5].(Fig. 2) In this dataset, Gli1-GFP⁺ cells were isolated by FACS from the molars of *Gli1*$^{GFP/+}$;*Pthrp-creER*;*R26R*^{tdTomato}mice at PN6, following a tamoxifen pulse at PN3. After unsupervised clustering, cell types were preliminarily annotated based on a published tooth cell atlas and established marker genes (e.g., *Pthlh* for dental follicle, *Sox9* and *Hhip* for apical papilla, *Wif1* for dental papilla)[5,6,25](Supplementary Fig. 1A). We observed that neither *Gli1* nor *Pthlh* expression alone could specifically define the dental follicle population (Fig. 2B, see the CellType annotation, and Supplementary Fig. 1A). Instead, *Grem2*, *Lepr*, and *Pthlh* marked distinct subsets within the dental follicle (Fig. 2B, See the SubCellType annotation, and supplementary Fig. 1B). Accordingly, we subset and renamed the dental follicle cells as three distinct subpopulations: Grem2⁺ DF, Lepr⁺ DF, and Pthlh⁺ DF (Fig. 2A). Dot plot analysis confirmed the specificity of the marker genes for each subcluster (Fig. 2B, See the SubCellType annotation).

Trajectory inference using Slingshot and Monocle2 revealed that Grem2$^+$ cells were positioned at the root (early stage) of the differentiation trajectory (Fig. 2C,D). Gene enrichment analysis of genes whose expression correlated with the trajectory pattern of Grem2 was performed (Fig. 2E). GO analysis of these genes highlighted significant enrichment for terms related to ossification, extracellular matrix organization, regulation of epithelial cell proliferation, mesenchymal development, connective tissue development, and mesenchymal cell differentiation (Fig. 2F,G). Collectively, these results indicate that Grem2$^+$ dental follicle cells represent a progenitor-like subpopulation with a potential role in directing osteogenic differentiation and tissue morphogenesis during tooth root development.

We next analyzed scRNA-seq data from PTHrP-mCherry$^+$ cells FACS-sorted from mandibular tissues at P6, P15, P25, and 8 weeks[33](Fig. 2H–L). Datasets were computationally integrated using Seurat[34]. Consistent with prior findings, *Grem2*, *Lepr*, and *Pthlh* again defined discrete dental follicle subpopulations. Notably, on UMAP visualization, the Grem2$^+$, Lepr$^+$, and Pthlh$^+$ cell subpopulations exhibited a complementary distribution pattern, collectively reconstituting the dental follicle population identified from PTHrP$^+$ FACS-sorted cells (Fig. 2L). DEG analysis was subsequently performed to compare Grem2$^+$ cells with Lepr$^+$ or Pthlh$^+$ cells. Relative to Lepr$^+$ cells, Grem2$^+$ cells were enriched in GO terms associated with cell growth regulation, cell–cell adhesion, and epithelial proliferation, suggesting a role in maintaining progenitor features and modulating epithelial–mesenchymal crosstalk (Fig. 2N). Furthermore, compared with Pthlh$^+$ cells, Grem2$^+$ cells displayed enrichment in GO terms related to ossification, epithelial proliferation, and extracellular matrix organization, pointing to a functional predisposition toward osteogenic differentiation and matrix remodeling during root development (Fig. 2O). Together, these analyses position Grem2$^+$ cells as a functionally distinct DFSC subpopulation with progenitor-like properties and osteogenic bias, complementary to Lepr$^+$ and Pthlh$^+$ subsets within the dental follicle.

Grem2$^+$ Cells Contribute to Interradicular Alveolar Bone, Periodontal Ligaments, and Cementum

The above scRNA-seq analyses suggested that Grem2$^+$ cells may function as a subset of dental follicle progenitor cells contributing to periodontal tissues during root development. To test this hypothesis, we generated a tamoxifen-inducible *Grem2*-CreERT2 knock-in mouse line by replacing the endogenous TGA stop codon with a “P2A-CreERT2” cassette using CRISPR/Cas9 technology. These mice were then crossed with Rosa26-tdTomato reporters, enabling precise labeling of Grem2$^+$ cells and their progeny upon tamoxifen induction (Fig. 3A). This approach allowed us to trace the fate of Grem2$^+$ cells over defined developmental windows.

We first performed a pulse-chase experiment from PN1.5 to PN3.5 to validate *Grem2* expression. TdTomato signals were predominantly localized to the root follicle, without overlapping with K14$^+$ epithelium (Fig. 3B), consistent with our In situ hybridization findings. This confirmed that tdTomato

signals reliably represent Grem2⁺ cells and their derivatives. Sparse tdTomato⁺ cells were also observed in the crown follicle and dental pulp.

To investigate the role of Grem2⁺ cells during molar root development, tamoxifen was administered intraperitoneally at PN3.5, and samples were harvested at PN5 (pulse-chase to label Grem2-expressing cells), PN15 (during root development), and PN28 (after root development completion [11]). EdU was injected 6 hours prior to harvest to label proliferating cells (Fig. 3C). Consistent with our previous in situ hybridization results, at PN5, Grem2⁺ cells were localized to the apical follicle of molars, abundantly distributed at the root-forming front (Fig. 3C,a2), with fewer cells at the root furcation region (Fig. 3C,a1). Specifically, Grem2⁺ cells were located beneath the level of the cementoenamel junction—the region at the enamel organ's cervical margin where the future crown and root meet (Fig. 3C, a3). EdU⁺ proliferating cells were observed at the root-forming front, including the dental follicle and apical papilla.

The number of Grem2⁺ descendant cells increased with molar root elongation (Fig. 3C, b-c). At PN15 and PN28, tdTomato⁺ cells gave rise to periodontal tissues, including the alveolar bone (especially interradicular alveolar bone), the periodontal ligament, and cementoblasts. At PN15, during active root development, EdU⁺ cells were widely distributed in the interradicular bone, PDL and the root-forming front (including apical dental follicle and apical papilla)(Fig. 3C,b1-b3). Grem2⁺/EdU⁺ cell number was increased and they were found in the alveolar bone and at the root-forming front, indicating that Grem2⁺ cells were highly proliferative at this stage (Fig. 3C,b1-b2).

At PN28, after root formation was complete (Fig. 3C,c), Grem2⁺ cells at PN3.5 contributed to 59.09 ± 13.58% of the PDLs and 36.29 ± 7.69% of the interradicular alveolar bone. EdU⁺ cells were predominantly localized in the bone marrow cavity of the alveolar cancellous bone and root apical, with sparse labeling in the cervical portion of interradicular bone and periodontal tissues, suggesting that the alveolar bone had achieved homeostasis (Fig. 3C,c1,c3). Nevertheless, Grem2⁺/EdU⁺ cells were still detected at the apical foramen (Fig. 3C, c2), indicating that Grem2⁺ cells continue to contribute to the maintenance of molar root homeostasis.

To further characterize the tissue contributions of Grem2⁺ cells, we performed immunostaining for dental markers in lineage-traced cells, including Runx2 for osteoblast/osteoprogenitor cells, Osterix (Osx) and osteocalcin (OC) for cementoblasts, and Periostin (POSTN) for PDLs (Fig. 3D). Immunostaining results indicated that Grem2⁺ cells overlap with these markers, indicating Grem2 + progenitors could differentiate into alveolar bone, PDLs, and cementoblasts. Collectively, these results establish Grem2⁺ DFSCs as a multipotent progenitor population that gives rise to the major periodontal tissues—interradicular alveolar bone, periodontal ligament, and cementoblasts—during molar root development.

Grem2⁺ Cells Exhibit Trilineage Differentiation Potential In Vitro

Trilineage differentiation capacity is a defining criterion for mesenchymal stem cells[35,36]. To evaluate the characteristics of Grem2$^+$ cells *in vitro*, we utilized *Grem2*-CreERT2; tdTomato mice and induced recombination at PN3.5. DFSCs were harvested at PN5.5 and cultured to passage 3. Grem2$^+$ cells constituted approximately 80% of the total DFSC population and could be expanded clonally *in vitro* (Fig. 4A, B). These cells co-expressed the mesenchymal stem cell markers CD90/Thy1, CD44, and CD29, while being negative for CD34, Sca1, and CD31[36] (Fig. 4C). Flow cytometry analysis of Grem2$^+$ cells further confirmed their CD44$^+$CD31$^-$ phenotype (Fig. 4D, E), consistent with the immunofluorescent staining results.

To assess their differentiation capacity *in vitro*, DFSCs were cultured to passage 3 in standard medium and then switched to chondrogenic, osteogenic, or adipogenic differentiation media[13]. Immunofluorescent staining demonstrated that Grem2$^+$ cells co-expressed the chondrogenic marker aggrecan (ACAN), the osteogenic marker Runx2, and the adipogenic marker Perilipin-1, confirming that Grem2$^+$ cells possess trilineage differentiation potential *in vitro* (Fig. 4F). Thus, Grem2$^+$ cells satisfy the essential criteria for mesenchymal stem cells: clonal expansion, expression of MSC surface markers, and trilineage differentiation capacity[36].

Grem2$^+$ Cells Persist into Adulthood and Respond to Tissue Regeneration

To determine whether Grem2$^+$ cells persist beyond root development and contribute to dental tissue regeneration in adulthood, we assessed their fate during early and late stages of root formation.

Tamoxifen was administered at PN5, marking the onset of root development, and analyses were conducted up to PN21, when root development is fully completed (Fig. 5A). Consistent with results obtained from tamoxifen administration at PN3.5, Grem2$^+$ cells were localized to the dental follicle at the root-forming front (traced from PN5 to PN7). Derivatives of Grem2$^+$ cells persisted in the periodontal tissues surrounding the root apices, contributing to the PDL, alveolar bone, and cementoblasts (traced from PN5 to PN21).

We then administered tamoxifen at PN14, when the root had reached approximately half its final length, and harvested mice at PN16 and PN21 (Fig. 5B). Traced from PN14 to PN16, tdTomato signals were detected in the periodontal tissue around the root apex, albeit at lower levels than those observed during the early stage (traced from PN5 to PN7). Notably, when traced from PN14 to PN21, Grem2$^+$ cells labeled at the late stage of root formation continued to increase in number and became distributed around the root apices as root elongation progressed, with sparse distribution within the alveolar bone. These findings indicate that Grem2$^+$ cells continuously contribute to the PDL, alveolar bone, and cementum throughout molar root elongation.

We further traced Grem2$^+$ cells and their progeny after root development was completed, from PN30 to PN35 (Fig. 5C). tdTomato signals remained detectable at the root apex and within the alveolar bone

(Fig. 5C, c1–c2), indicating that Grem2⁺ cells are not merely a transient population confined to the developmental period. Rather, they appear to retain self-renewal and differentiation potential into adulthood. These findings suggest that Grem2⁺ cells represent a population of adult stem or progenitor cells residing in the apical region, playing a crucial role in maintaining periodontal tissue homeostasis and facilitating injury repair.

To evaluate whether Grem2⁺ cells contribute to interradicular alveolar bone repair following injury, we created a defect at the most cervical ridge of the interradicular alveolar bone of the lower first molar on one side in 6-week-old *Grem2*-CreERT2; tdTomato mice, using the contralateral side as a control. Mice were traced for three weeks post-injury (Fig. 5D). The results showed that tdTomato⁺ cells increased in number at both the interradicular alveolar bone and the root apex, indicating that injury to the interradicular bone accelerates the recruitment of Grem2⁺ cells to the site of repair (Fig. 5E). These findings confirm that Grem2⁺ cells function as adult stem cells contributing to alveolar bone homeostasis and injury repair.

Grem2⁺ DFSCs determine interradicular Alveolar Bone Development and tooth root morphogenesis

To further investigate the role of Grem2⁺ DFSCs in tooth development, we cross-bred *Grem2*-CreERT2 mice with Rosa26-DTA mice. In this system, tamoxifen administration removes the stop codon upstream of DTA, leading to DTA expression that is cytotoxic to Grem2⁺ cells. Since induction at PN3.5 resulted in lethality, we administered tamoxifen at PN9, when the mice are larger and the molar root is partially developed, and reduced the tamoxifen dosage to minimize mortality (Fig. 6A). Micro-CT analysis revealed that, in *Grem2*-CreERT2; DTA/+ mice, the mesial and distal root apices of the first molar were positioned closer together, appearing nearly parallel (Fig. 6C-E), whereas wild-type controls exhibited a divergent root configuration (Fig. 6B). Comparison of the root-to-crown width ratio between WT and *Grem2*-CreERT2; DTA/+ mice showed a significant decrease following Grem2⁺ cell ablation (Fig. 6F,G). Although the morphological changes were mild upon histological examination ((Fig. 6H,I)), we observed increased bone density at the cervical portion of the interradicular bone in *Grem2*-CreERT2; *DTA*/+ mice (Fig. 6J,K). Moreover, osteogenic activity at the same region was decreased, as demonstrated by Sp7 immunostaining (Fig. 6L, M).

GREM2 is a secreted extracellular protein and a known antagonist of BMP signaling[37,38]. To evaluate the role of GREM2 secreted by Grem2 + cells on tooth development, we generated *Grem2* knock-in mice using CRISPR-Cas9 technology targeting exon 2 (Fig. 7A). A previous study reported that *Grem2*-KO mice exhibited smaller body size and mandibles[18]; however, we did not observe significant differences in body size between *Grem2*-KO and control mice until postnatal 10 month. Notably, we observed short and sharpened incisor phenotype in the KO group in young mice, and short incisor grinded to the gingival level in older mice at 10 month in our research (data not shown), which was consistent with previous findings[18,39].

We evaluated molar development by micro-CT at PN15 and PN90 (Fig. 7B). In *Grem2*-KO mice, root and interradicular alveolar bone development was retarded, as evidenced by shorter roots and reduced interradicular alveolar bone at PN15(Fig. 7B, a-d). These differences became more pronounced by PN90. Alveolar bone volume under the root furcation decreased, whereas bone density increased in *Grem2*-KO mice. Moreover, the crown-to-root length ratio increased, accompanied by an enlarged pulp chamber volume (Fig. 7B, e-h). However, the molar eruption and total tooth length was less affected (Fig. 7B, i-j). Of note, although interradicular alveolar bone volume was reduced in *Grem2*-KO mice, the interseptal bone volume between the first and second molars remained less affected.

To further explore the effects of *Grem2* knockout on root morphogenesis, we compared serial morphological changes during root development between WT and *Grem2*-KO mice (Fig. 7C). In WT mice, crown, root, and alveolar bone development proceeded in a coordinated manner. In *Grem2*-KO mice, crown formation was unaffected at PN4; however, by PN7, root and alveolar bone development were delayed. The epithelial diaphragm of the first molar had formed in WT mice but was absent in *Grem2*-KO mice. At PN14, the crown-to-root ratio had reached 1:1 in WT mice; in contrast, KO mice exhibited a markedly increased crown pulp height and reduced root length, accompanied by decreased interradicular alveolar bone formation. By PN21, when root development was nearly complete, *Grem2*-KO mice displayed a narrowed root furcation with reduced alveolar bone volume beneath, a phenotype resembling but more severe than that observed in *Grem2*-CreERT2; DTA mice. Additionally, the crown pulp chamber height remained enlarged in *Grem2*-KO mice. Masson staining confirmed a reduction in interradicular alveolar bone volume alongside an increase in bone density (Fig. 7D,E). In WT mice, the furcation alveolar bone exhibited typical cancellous bone architecture with abundant trabeculae, whereas in KO mice, it appeared dense with sparse trabeculae at the base of the alveolar bone.

Given that Grem2$^+$ cells contribute to periodontal tissues including alveolar bone, PDL, and cementoblasts, we investigated whether *Grem2* knockout affects periodontal tissue development. Results showed osteogenic capacity was impaired following *Grem2* knockout, as evidenced by reduced Osterix expression in the interradicular alveolar bone of KO mice (Fig. 7F,a-b). Ocn expression was also decreased in *Grem2*-KO mice, indicating impaired cementoblast generation (Fig. 7F, c,d). However, Masson staining at PN21 revealed increased cellular cementum in *Grem2*-KO mice, a finding corroborated by H&E staining at 6 weeks (Fig. 7D,E). The PDL develop was also compromised in Grem2-KO mice, which was confirmed by periostin immunofluorescence staining (Fig. 7F,e-f). However, at 6 weeks, The PDL appeared largely unaffected, except for a widened PDL space in KO mice. Sirius red staining also showed widened PDL space and more condensed PDL fibers in *Grem2*-KO mice (Fig. 7F,e-f, and Fig. 7G).

Taken together, these findings demonstrate that Grem2$^+$ DFSCs secreting GREM2 play an essential role in molar root morphogenesis by regulating periodontal tissue development, particularly the formation of the interradicular alveolar bone. Ablation of Grem2$^+$ DFSCs affected tooth root morphogenesis; Grem2 deficiency impaired periodontal development, resulting in decreased alveolar bone volume, increased bone density, enhanced cellular cementum deposition, and widened PDL space.

Grem2 knockout impairs interradicular alveolar bone turnover

To elucidate how Grem2 deficiency reduces interradicular alveolar bone, we assessed both osteogenic and osteoclastic activities during molar root development. In Grem2-KO mice, osteogenesis was significantly decreased, as shown by reduced ALP staining (Fig. 8A) and diminished expression of Runx2 and Sp7 (immunofluorescence) (Fig. 8B). Meanwhile, osteoclastic resorption was also compromised, evidenced by weaker TRAP staining (Fig. 8C). Together, these results indicate that Grem2 knockout disrupts the normal turnover of interradicular alveolar bone during molar development.

We next investigated whether Grem2 knockout affects stem cell activity. To label quiescent (label-retaining) cells, EdU was administered three times between PN3.5 and PN5.5, followed by a 7-day chase (Fig. 8D,a). At PN12.5, the number of EdU-retaining cells was markedly lower in Grem2-KO mice, suggesting an early loss of quiescent stem cells (Fig. 8D, b-e). Additionally, proliferating cells were examined by EdU injection 6 h before sacrifice (Fig. 8E,a). Although the proliferation rate decreased significantly in KO group. Moreover, the spatial distribution changed notably: at PN15, EdU^+ cells in Grem2-KO mice were confined to the most apical region of the interradicular bone, whereas in wild-type mice they were evenly distributed throughout the cervical portion (Fig. 8E, b-e). These findings imply that Grem2 deletion reduces the pool of quiescent stem cells and alters the recruitment of DFSCs toward the cervical aspect.

$Grem2^+$ DFSCs Mediate Intercellular Communication Through the IGF Signaling Axis

Stem cells reside in specialized niches and are regulated by niche factors through autocrine and paracrine signaling[7]. In humans, mutations in *GREM2* cause microdontia, suggesting that the rhythm of tooth development may be affected. However, the total molar tooth volume in our *Grem2* knockout model was not significantly altered, pointing to the involvement of additional signaling pathways regulating this tooth phenotype.

To further investigate the stem cell microenvironment of the root follicle, we performed CellChat analysis. To gain insights into potential signaling interactions among different cellular domains within the dental mesenchyme, we analyzed the P3.5 scRNA-seq dataset as a representative time point (Fig. 9A,B). ncWNT, IGF, ANGPTL, PTH, and IGFBP signaling were most enriched among the outgoing signals of the root follicle, while PTH, SLITRK, ANGPTL, and IGF signaling were most enriched among incoming signals (Fig. 9A). Unsupervised clustering of outgoing signaling revealed that the root follicle exhibits a unique paracrine profile, characterized by enrichment in IGF, PTH, and IGFBP signaling (Fig. 9B). PTH signaling has been previously reported to regulate molar eruption[7], but we found tooth eruption were unaffected after Grem2 disability. Here, we focused on IGF signaling, as pathway network analysis confirmed that the root follicle subgroup is the major source of IGF signaling within the dental

mesenchyme and IGF signaling was predicted to mediate interactions between root follicle cells and other cellular domains (Fig. 9C).

IGF ligands include IGF1 and IGF2[40]. Previous studies have shown that both *Igf1* and *Igf2* are expressed in the dental follicle, as evidenced by scRNA-seq and In situ hybridyzation in situ staining[6]. In situ hybridyzation staining revealed that *Igf2* exhibited higher expression levels than *Igf1*[6]; however, *Igf2* was barely detectable by scRNA-seq. This discrepancy may be partly attributed to the fact that *Igf2* is an imprinted gene, whose expression depends on the paternal allele through epigenetic regulation[40,41].

To determine whether IGF2 plays a functional role in Grem2$^+$ dental follicle cell development, we first examined its expression in Grem2$^+$-derived cells. Immunofluorescence staining revealed that IGF2 was expressed in cementoblasts, alveolar bone, and periodontal ligament. Notably, IGF2 colocalized with tdTomato$^+$ cells most prominently at the root furcation, involving both interradicular alveolar bone and PDL (Fig. 9D, a). In contrast, such colocalization was rarely observed in the interseptal alveolar bone between the first and second molars (Fig. 9D, b).

To further investigate whether IGF2 signaling acts downstream of Grem2, we compared IGF2 expression between PN14 WT and *Grem2*-KO mice (Fig. 9E). Strikingly, IGF2 expression was absent in the interradicular alveolar bone of *Grem2*-KO mice (Fig. 9E, b1), whereas its expression in the interseptal alveolar bone between the first and second molars was only slightly reduced (Fig. 9E, b2). This differential expression pattern may explain why *Grem2*-KO mice exhibit reduced alveolar bone volume specifically under the root furcation, but not between the first and second molars.

To further validate that IGF2 mediates the function of Grem2$^+$ cells and that its loss contributes to the molar phenotypes observed in *Grem2*-KO mice, we cross-bred *Grem2-CreERT2* mice with *Igf2*-flox mice and administered tamoxifen at PN3.5. Samples were harvested at PN28. Micro-CT analysis revealed smaller lower first molars in *Grem2-CreERT2; Igf2*$^{flox/-}$mice (Fig. 9F, a-e). The mesial root was shortened, and the root furcation alveolar bone volume was reduced, partially recapitulating the molar phenotype of *Grem2*-KO mice. H&E staining pointed this difference to decreased cementoblasts (Fig. 9F, f-g) Collectively, these results indicate that IGF2 acts downstream of Grem2 and that Grem2$^+$ cells exert their normal functions through IGF2-mediated signaling.

Discussion

In this study, we characterized a novel population of Grem2$^+$ DFSCs that play a critical role in postnatal alveolar bone development and tooth morphogenesis. Through scRNA-seq reanalysis and lineage tracing, we are the first to identify Grem2$^+$ cells as a specific marker of DFSCs and as the cellular origin of the periodontium, including alveolar bone, periodontal ligament (PDL), and cementum. Moreover, Grem2$^+$ cells persist into adulthood and can participate in alveolar bone repair. Ablation of Grem2$^+$ cells, conventional knockout of *Grem2*, or diminished Igf2 secretion from Grem2$^+$ cells all affected molar morphologies. Importantly, we report for the first time a marked reduction in interradicular alveolar bone

volume, a severely narrowed molar root furcation, and an enlarged pulp chamber in *Grem2*-knockout mice. These defects-reduced alveolar bone and molar dysmorphology-were caused by disrupted DFSC homeostasis and decreased alveolar bone turnover. Our findings directly elucidate the mechanism by which human *GREM2* deficiency leads to dental developmental anomalies, including taurodontism and short roots. Collectively, this study bridges a critical knowledge gap in DFSC identification and offers mechanistic insights into the pathogenesis of tooth developmental anomalies, laying a foundation for future exploration of regenerative strategies targeting alveolar bone.

Grem2 has been reported as a candidate gene for tooth agenesis, highlighting its essential role in tooth development[16–18]. In humans, *GREM2* (OMIM *608832)* mutations have been associated with a range of dental anomalies, including tooth agenesis (TA), microdontia, taurodontism, and short tooth roots[16,17]. However, the mechanisms by which *GREM2* mutations lead to these anomalies remain unclear. Similarly, *Grem2*-deficient mice (*Grem2*$^{-/-}$) exhibit defective incisor morphogenesis, with markedly reduced incisor length and wear extending to the gum line[18]. However, the molar phenotype had not been described in previous studies. Although the gross morphology of the molar crown was reported to be normal, whether *Grem2* deficiency affects root development—an aspect more closely aligned with the human anomalies—had not been investigated[18].

In this context, our study contributes an important piece to the overall understanding of tooth development by revealing that Grem2^{+} cells represent a population of dental follicle stem cells that give rise to the periodontium, particularly the interradicular alveolar bone. Grem2 deficiency impaired interradicular alveolar bone formation, resulting in a narrowed root furcation. Both of these phenotypes recapitulate the taurodontism observed in humans carrying *GREM2* mutations.

The identification of Grem2^{+} DFSCs provides a novel and specific *in vivo* lineage tracing marker, enriching the toolkit for studying dental follicle stem cell heterogeneity. Compared with previously characterized markers such as PTHrP and Lepr, Grem2 exhibits several distinct advantages that highlight its unique role in root development. A key distinction lies in spatial specificity: while PTHrP and Lepr label both the coronal and root follicles of molars before eruption[6,7], Grem2^{+} cells exclusively mark the root follicle, enabling precise targeting of the root-associated dental follicle without confounding contributions from the crown region. This specificity is further reflected in their contribution pattern to the interradicular alveolar bone. PTHrP^{+} and Lepr^{+} cells are largely confined to the cervical portion[5–7], whereas Grem2^{+} cells contribute to both the cervical and basal portions, indicating a broader and more complete engagement with this critical periodontal structure. Moreover, single-cell RNA-seq analysis revealed that Grem2^{+} DFSCs are transcriptionally distinct from and more primitive than PTHrP^{+} and Lepr^{+} cells, a primed state that likely accounts for their greater contribution to the interradicular bone compartment and broader differentiation potential. Notably, as root elongation proceeds, Grem2^{+} cells become progressively restricted to the apical region while continuing to supply periodontal tissues throughout root development—a dynamic behavior that aligns with the ongoing demands of root growth and suggests a sustained progenitor function at the root apex. Together, these features establish Grem2

as a highly specific and functionally relevant marker for a distinct DFSC subpopulation that plays a central role in interradicular alveolar bone formation and root morphogenesis, complementing and extending the existing repertoire of dental follicle stem cell markers.

Taking advantage of lineage tracing of Grem2^{+} cells, this study further demonstrated that Grem2^{+} dental follicle cells persist into adulthood and contribute to alveolar bone injury repair, thereby providing another potential endogenous cellular target for regenerative therapies of alveolar bone lesions.[5,12,13,42].

More importantly, lineage tracing of Grem2^{+} cells and the *Grem2*-knockout mouse model offer new insights into the etiology of tooth agenesis caused by *GREM2* mutations in humans. Human carriers of the *GREM2* p.Gln76Glu variant exhibit hypodontia with associated dental anomalies, including taurodontic maxillary molars [16,17]. The residual p.Gln76 is a highly evolutionarily conserved amino acid located in the central part of the GREM2 domain, which contains a cysteine-knot structural motif critical for proper protein folding, dimerization, and interaction with BMP receptors[16,17,43]. The p.Gln76Glu mutation generates a hypermorphic allele with increased inhibitory activity, which could lead to enhanced inactivation of BMP2 and BMP4[44]. The *Grem2* knockout mouse model (exon 2 deletion) in this study recapitulated the taurodontic phenotype. In addition, *Grem2*-KO mice showed delayed appearance of the epithelial diaphragm, reduced interradicular alveolar bone volume but increased bone density, and decreased turnover of interradicular bone.

Organ structure formation and maintenance rely on signaling networks that govern cell fate in a context-dependent manner[21,45]. BMP signaling regulates differentiation, apoptosis, and proliferation in a concentration-dependent fashion[21], and cells sense spatial position by interpreting local BMP gradients, which are shaped by the action of BMP inhibitors[46]. Given that Grem2 is a known BMP antagonist, and previous studies have shown that Grem2 inactivation enhances osteoblast differentiation (e.g., elevated *Alp*, *Osteocalcin*, and *Osterix* mRNA upon BMP-2 stimulation) [37,47], we propose the following model: Grem2-expressing cells secrete Grem2 into the DFSC niche, where it functions to maintain stemness by fine-tuning the balance between proliferation and differentiation (Fig. 10A). Loss of Grem2 leads to excessive BMP signaling within the niche, causing premature exhaustion of DFSCs and accelerated differentiation of progenitor cells. Consequently, the bone turnover rate declines, manifesting as decreased interradicular alveolar bone remodeling (Fig. 10B). This model parallels the role of another BMP antagonist, Grem1, in regulating villus length along the small intestine through a gradient of BMP activity[46]. In the proximal intestine, high Grem1 expression suppresses BMP signaling, reducing apoptosis and promoting proliferation, resulting in longer villi; conversely, lower Grem1 expression in the distal intestine permits stronger BMP signaling, which promotes apoptosis and inhibits proliferation, yielding shorter villi[46]. Thus, both Grem1 and Grem2 exemplify how BMP antagonists shape tissue architecture by modulating local signaling gradients.

Specifically, the underlying mechanism involves multiple interrelated aspects. First, *Grem2* knockout compromised the number of dental follicle stem cells, reducing the progenitor pool available for

periodontal and alveolar bone formation. The decreased EdU retaining cells during molar development give the clue. Second, loss of secreting Grem2 elevated the local BMP signaling gradient, leading to premature differentiation of remaining progenitors and consequently depleting the stem cell reservoir. Third, the reduced bone turnover in *Grem2*-KO mice likely results from a combination of diminished osteoclast activity and altered osteoblast–osteoclast coupling. Under physiological conditions, BMP signaling fine-tunes the RANKL/OPG axis, which governs osteoclastogenesis. Disruption of the BMP gradient by Grem2 deficiency may shift this balance, suppressing osteoclast recruitment and activation. Concurrently, the premature differentiation of osteoblasts leads to the deposition of dense, poorly remodeled bone with reduced trabecular architecture. The net effect is a state of low bone turnover, characterized by decreased bone volume, increased mineral density, and sparse trabeculae—features consistent with the Masson staining observations in our study. Collectively, these three mechanisms—stem cell depletion, premature differentiation, and impaired bone remodeling—act in concert to produce the decreased interradicular bone defects seen in *Grem2*-deficient mice.

Interestingly, root length remained less affected in *Grem2*-knockout mice, with the phenotype confined to the periodontium, particularly the interradicular alveolar bone. This contrasts sharply with the disruption of BMP signaling in Gli1$^+$ MSCs, where *Gli1-CreER; Bmpr1a*$^{fl/fl}$mice lacked any identifiable root structure despite an apparently normal crown–root transition[11]. Similarly, perturbation of Wnt, Hedgehog, TGF-β, and FGF signaling also caused severe root defects[48–50]. This phenotypic discrepancy likely stems from several interrelated factors. A key distinction lies in the differential contribution weights of the targeted cell lineages. Gli1$^+$ cells function as the principal MSC population driving molar root growth, with their progeny contributing to virtually all root structures, including dentin, dental pulp, cementum, periodontal ligament, and surrounding alveolar bone[11]. In contrast, Grem2$^+$ cells constitute a distinct subpopulation within the dental follicle that partially overlaps with Gli1$^+$ cells and primarily regulates MSC homeostasis and interradicular alveolar bone formation. Furthermore, the nature of the genetic intervention differs fundamentally. *Bmpr1a* ablation directly eliminates BMP receptor signaling within Gli1$^+$ core progenitors, thereby preventing the initiation of odontogenic differentiation altogether. *Grem2* deficiency, by comparison, attenuates BMP antagonism, resulting in signaling gradient imbalance rather than complete pathway paralysis[22,46]. Given that precise BMP signaling dosages and spatial gradients are essential for proper developmental patterning[22,23,46], Grem2—as a specific antagonist of BMP2 and BMP4—appears to fine-tune rather than drive core developmental programs. Consequently, *Grem2* knockout manifests as reduced interradicular alveolar bone and taurodontism-like root morphology, rather than complete root agenesis.

It's well accepted that delayed activation of the epithelial diaphragm led to an apically positioned root furcation in mouse molars, a morphology resembling taurodontism[2,50]. In this study, the onset of epithelial diaphragm formation was significantly delayed in *Grem2*-knockout mice, resulting in an enlarged coronal pulp chamber. These findings suggest that loss of Grem2 disrupts local BMP gradient thus impaired early epithelial–mesenchymal interactions, specifically affecting the timing of epithelium diaphragm initiation, leading to apically displaced epithelial diaphragm, causing an enlarged pulp

chamber and taurodontoid furcation. Notably, root elongation and interseptal bone were relatively preserved in *Grem2*-KO mice. Given that the primary driver of root lengthening is the HERS–papilla axis[1,2], this observation implies that HERS segments contacting the lateral dental follicle—where Grem2 function is less prominent—are less affected by Grem2 deficiency. In contrast, the HERS at the root furcation (i.e., the epithelial diaphragm), which contacts the furcation dental follicle where Grem2$^+$ cells are enriched and Grem2 function is more pronounced, is more severely disturbed. This spatial dichotomy further supports the notion that Grem2$^+$ cells exert their regulatory function in a spatially restricted manner, preferentially targeting the interradicular region rather than the entire alveolar bone complex. This conclusion is consistent with our lineage tracing data, which demonstrated a preferential contribution of Grem2$^+$ cells to interradicular bone over interseptal bone.

Meanwhile, the identification of Igf2 as a paracrine factor secreted by Grem2$^+$ dental follicle cells provides mechanistic insight into how this subpopulation influences overall tooth size, including the volume of interradicular bone. Of note, the mandible and molar sizes of *Grem2*-KO mice in our study were unaffected, whereas *GREM2* mutations in humans cause microdontia and *Grem2*^{tm1Lex} mutant mice develop micrognathia[17] and the the *Grem2*^{tm1Lex} mutation in mice caused small mandible[18]. One possible explanation is that Igf2 functions downstream of Grem2, as evidenced by the diminished Igf2 expression beneath the root furcation in *Grem2*-KO mice. Additionally, the dominant-negative effect of the *Grem2*^{tm1Lex} allele may globally impair Grem2$^+$ cell function and compromise their growth factor secretion, contributing to the broader craniofacial phenotype. However, the precise regulatory mechanism underlying these observations requires further investigation.

Nevertheless, several limitations of this study should be acknowledged. Although the conventional *Grem2* knockout mouse model recapitulates human mutation, the observed phenotypes may be confounded by systemic effects. A more refined approach would involve conditional knockout of *Grem2* under tissue-specific promoters to dissect its cell-autonomous functions. Furthermore, to investigate the autocrine effects of Grem2, a *Grem2*-CreERT2; *Grem2*$^{flox/flox}$; R26-TdTomato triple-transgenic line would ideally be required to trace Grem2$^+$ cells following *Grem2* inactivation. However, because the *Grem2*-CreERT2 allele was generated using a knock-in strategy, we were unable to generate this line, which represents a technical constraint of the current study.

Taken together, this work identifies Grem2 as a specific marker for root dental follicle stem cells and provides mechanistic insight into tooth dysmorphology caused by *Grem2* mutations. These findings lay the groundwork for future studies aimed at elucidating the precise regulation of Grem2 in DFSC maintenance and interradicular alveolar bone regeneration. The persistence of Grem2$^+$ DFSCs into adulthood and their active contribution to injury repair position them as a promising endogenous cellular target for alveolar bone regeneration. Thus, this work not only advances our understanding of the cellular basis of root development but also opens potential therapeutic avenues for restoring periodontal support in patients with advanced bone loss.

Materials and methods

Animals

All animal studies were approved by the Animal Ethics Committee of the Affiliated Stomatology Hospital of Tongji University ([2022]-DW-11) and conducted in accordance with the NIH Guide for the Care and Use of Laboratory Animals. *Grem2*-knockout and *Grem2*-CreERT2 mice were custom-generated by Cyagen Biosciences (Shanghai, China). *Igf2*$^{fl/+}$, Rosa-LSL-tdTomato, Rosa26-EGFP-DTA, and C57BL/6 mice were purchased from the same vendor and maintained on a C57BL/6 background. All mice were housed under specific pathogen-free (SPF) conditions (23 ± 2°C, 55 ± 5% humidity, 12:12 h light/dark cycle) with food and water provided *ad libitum*. Noon of the day on which a vaginal plug was detected was designated as embryonic day 0.5 (E0.5). Both male and female mice were used, as no sex-dependent differences were observed.

Genotyping was performed by PCR using genomic DNA extracted from tail biopsies. Briefly, tail samples (~ 2 mm) were digested in 180 µL of 50 mM NaOH at 95°C for 30 min, neutralized with 20 µL of 1 M Tris-HCl (pH 8.0), and centrifuged. The supernatant was used as template DNA. Positive, negative, and no-template controls were included in each PCR run. PCR products were resolved by agarose gel electrophoresis.

All surgical procedures were performed under anesthesia with 1.25% tribromoethanol (Beijing Jitian Biotechnology). Mice were euthanized by an overdose of tribromoethanol at the experimental endpoint.

Re-analysis of scRNA-seq data

ScRNA-seq data were obtained from the GEO database (GSE189381 for serial molar development; GSE237439 for Gli1^{+} cells; GSE313714 and GSE120108 for PTHrP^{+} cells). Analyses were performed using Seurat (version 4.4.0) and R (version 4.4.3). Cell clusters were visualized using Uniform Manifold Approximation and Projection (UMAP). SingleR packages and published markers were used to identify dental mesenchymal subpopulations in the mouse molar. Pseudotime and differentiation trajectories were constructed using Monocle2 and Slingshot. Gene Ontology (GO) enrichment analysis was performed using ClusterProfiler. CellChat was implemented within Seurat to evaluate potential cell–cell interactions in the P3.5 dataset. All downstream analyses were performed using raw count data.

Lineage Tracing

Tamoxifen (HY-13757A, MCE) was dissolved in absolute ethanol at 55°C for 1 hour, then mixed with corn oil (HY-Y1888, MCE) to a final concentration of 20 mg/mL and incubated at 37°C overnight with shaking. The working solution was stored at − 20°C until use. For mice under 4 weeks of age, a single intraperitoneal injection of tamoxifen was administered at 1.0 mg/10 g body weight. For adult mice, the dose was increased to 1.2 mg/10 g body weight. Tamoxifen was administered at specified time points according to the experimental design.

Mandibles were collected at designated time points and fixed in 4% paraformaldehyde (PFA) overnight at 4°C. Following decalcification in 10% EDTA and cryoprotection in graded sucrose solutions, 10 μm frozen sections were prepared. Sections were subjected to immunostaining with specific antibodies, followed by imaging analysis.

EdU Administration

EdU (Beyotime, ST067) was dissolved in DMSO (KA1385, Kingmorn) at a concentration of 20 mg/mL and stored at − 20°C until use. Young mice received EdU via intraperitoneal injection at 0.60 mg/10 g body weight, whereas adult mice received a fixed dose of 1.0 mg per mouse. EdU was administered at the indicated time points prior to sacrifice, according to the experimental design.

Histology

For cryosectioning, samples were fixed in 4% PFA for 24 hours and decalcified in 10% RNase-free EDTA until the mandibles could be easily penetrated by a thin needle. They were then dehydrated sequentially in 15% sucrose for 24 hours and 30% sucrose for 24 hours at 4°C. Dehydrated samples were embedded in OCT compound (Tissue-Tek, Sakura) and stored at − 80°C until use. Cryosections were cut at 11 μm thickness using a cryostat (Leica) and stored at − 80°C.

For paraffin sectioning, samples were fixed and decalcified as described above, then dehydrated through a graded ethanol series (50%, 70%, 80%, 90%, and 100%) followed by xylene at room temperature. After embedding in paraffin, samples were sectioned at 4 μm thickness using a microtome (Leica).

For histological staining, paraffin sections were used for histological analyses. Hematoxylin and eosin (H&E) staining was performed according to the manufacturer's protocol. Modified Sirius Red staining (Solarbio, G1472) was used to assess type I and III collagen fibers in the periodontium. Masson's trichrome staining (Solarbio, G1340) and alkaline phosphatase (ALP) staining (Beyotime, P0321S) were performed to evaluate osteoblast activity. Tartrate-resistant acid phosphatase (TRAP) staining was performed using an Acid Phosphatase Kit (Sigma-Aldrich, 387A-1KT) to assess osteoclast activity.

For EdU detection, paraffin and cryosections were prepared as described above and stained using the EdU Cell Proliferation Kit with AF488 (Beyotime, C0071S) according to the manufacturer's instructions.

Immunostaining

Both cryosections and paraffin sections prepared as described above were used for immunofluorescence analysis. Paraffin sections were first deparaffinized. All sections were then rehydrated and permeabilized with 0.1% Triton X-100 in PBS for 10 minutes at room temperature. After blocking with 3% BSA for 1 hour, sections were incubated overnight at 4°C with primary antibodies, including rabbit anti-Osterix monoclonal antibody (1:100, Abcam, ab209484), rabbit anti-Periostin polyclonal antibody (1:200, Proteintech, 19899-1-AP), rabbit anti-IGF2 monoclonal antibody (1:100, Abmart, T56581), rabbit anti-Osteocalcin polyclonal antibody (1:200, Affinity, DF12303), and rabbit anti-RUNX2 polyclonal antibody (1:150, Affinity, AF5186). Sections were then incubated with CoraLite488-

conjugated goat anti-rabbit IgG (1:500, Proteintech, SA00013-2) or Alexa Fluor 594-conjugated donkey anti-rabbit IgG (1:500, Yeasen, 34212ES60) for 1 hour at room temperature. Nuclei were counterstained with DAPI (Beyotime, C1006).

In Situ Hybridization

In situ hybridization was performed on paraffin sections using a General RNA Fluorescent Detection Kit (PinpoRNA, PIF1000) with probes targeting *Grem2* (#1). mRNA detection was carried out according to the manufacturer's protocol. Images of histological analysis, immunostaining, and in situ hybridization were captured using a fluorescence microscope (Nikon).

Micro-CT Analysis

Mouse mandibles were collected and fixed in 4% PFA for 24 hours. Micro-CT images were acquired using a MicroCT 50 scanner (Scanco Medical, Switzerland) set to 70 kVp and 124 μA, with a slice resolution of 10 μm. Measurements, including bone volume fraction (BV/TV), root length, crown-to-root ratio, and total volume (TV), were analyzed using SCANCO evaluation software. Three-dimensional reconstructions were performed using iMaris 9.0 (Bitplane), and molar reconstruction and overlay were performed using 3D Slicer 5.10.0.

Primary Cell Culture

Grem2-CreERT2; tdTomato mice were administered tamoxifen at PN3.5. Dental follicle mesenchymal tissues from the first mandibular molars were harvested at PN5.5, minced into small fragments, and digested with 2.5 mg/mL type I collagenase (Thermo Fisher Scientific, 17100017) at 37°C for 30 minutes to obtain single-cell suspensions. Cells were cultured in α-MEM (Thermo Fisher Scientific, C12571500BT) supplemented with 10% FBS (Excell, FSD500) and 1% penicillin/streptomycin (Hyclone, SV30010) at 37°C in a humidified incubator with 5% CO_2. The medium was changed every 2 days, and cells were passaged upon reaching 80–90% confluence. DFSCs at passage 2 were used for all experiments.

Trilineage Differentiation

DFSCs were seeded at a density of 2×10^4 cells/cm² in 6-well culture plates. Trilineage differentiation was induced using osteogenic (Oricell, MUXMX-90021), chondrogenic (Oricell, MUXMX-90041), and adipogenic (Oricell, MUXMX-90031) differentiation media according to the manufacturer's protocols. After induction, osteogenic and adipogenic differentiated DFSCs were fixed in 4% PFA for 30 minutes. Chondrogenic pellets were collected, fixed in 4% PFA for 24 hours, dehydrated in 30% sucrose solution, embedded in OCT (Tissue-Tek, Sakura), and sectioned at 11 μm thickness. Immunofluorescence staining was performed using rabbit anti-RUNX2 polyclonal antibody (1:200, Affinity, AF5186), rabbit anti-Aggrecan polyclonal antibody (1:200, Affinity, DF7561), rabbit anti-Perilipin polyclonal antibody (1:100, Proteintech, 27716-1-AP), and CoraLite488-conjugated goat anti-rabbit IgG (1:500, Proteintech, SA00013-2).

Flow Cytometry

Passage 2 DFSCs were detached using trypsin/EDTA solution (Thermo Fisher Scientific, R001100). Single-cell suspensions were stained following the standard protocol of the Mouse Mesenchymal Stem Cell Surface Marker Assessing Kit (Oricell, MUXMX-09011). Flow cytometry was performed using a BD LSR Fortessa (BD, USA), and data were analyzed using FlowJo software (Treestar, v10.8.1).

Root-Furcation Drill-Hole Surgery

Mice were anesthetized by intraperitoneal injection of 1.25% tribromoethanol solution (0.269 mg/g body weight, JT0781, Beijing Jitian Biotechnology). A 22G (0.7 × 25 mm) hypodermic needle was used to gently perforate the buccal alveolar bone and create a defect in the cervical one-third of the interradicular alveolar bone of the left mandibular first molar. The contralateral right mandible was left untreated to serve as an internal control. Bilateral mandibular samples were collected and fixed in 4% paraformaldehyde for subsequent analyses.

Statistical Analysis

Statistical analysis was performed using GraphPad Prism 10.0 (GraphPad Software, USA). All data are presented as mean ± SD, with at least three biological replicates per group. Data normality was assessed using the Shapiro–Wilk test. Comparisons between two groups were made using the unpaired Student's t-test. For the interradicular bone injury assay, a paired Student's t-test was used. For experiments involving two independent variables, two-way ANOVA followed by Bonferroni's post hoc test was performed. A P value < 0.05 was considered statistically significant. Significance levels are denoted as follows: $P < 0.05$, *$P < 0.01$, and **$P < 0.001$.

Declarations

Acknowledgement:

The authors thank Dr Xiaofang Wang and Jiqiu Wang for help in experimental design and manuscript revision. The authors acknowledge the financial support of the National Natural Science Foundation of China (32300706) awarded to C.D. and Shanghai Pujiang Program (grant no. 23PJ1414200) to C.D.

Conflict of interests:

The authors declare no conflict of interests.

Contributions:

Q.Z. contributed to study design, data acquisition, analysis, and interpretation, and drafted the manuscript. Y.Y. contributed to conception, study design, and data interpretation. J.B. contributed to three-dimensional reconstruction and analysis of micro-CT images. Z.X. contributed to the analysis of Micro-CT images and data interpretation. Y.L. contributed to study design and critically revised the

manuscript. C.D. contributed to study design, manuscript drafting, and critical revision. All authors approved the final version and agreed to be accountable for all aspects of the work.

References

1. Li, J., Parada, C. & Chai, Y. Cellular and molecular mechanisms of tooth root development. *Development* 144, 374–384 (2017). https://doi.org/10.1242/dev.137216
2. Rao, P., Jing, J., Fan, Y. & Zhou, C. Spatiotemporal cellular dynamics and molecular regulation of tooth root ontogeny. *Int J Oral Sci* 15, 50 (2023). https://doi.org/10.1038/s41368-023-00258-9
3. Zhang, D. *et al.* LepR-Expressing Stem Cells Are Essential for Alveolar Bone Regeneration. *J Dent Res* 99, 1279–1286 (2020). https://doi.org/10.1177/0022034520932834
4. Kaku, M., Akiba, Y., Akiyama, K., Akita, D. & Nishimura, M. Cell-based bone regeneration for alveolar ridge augmentation–cell source, endogenous cell recruitment and immunomodulatory function. *J Prosthodont Res* 59, 96–112 (2015). https://doi.org/10.1016/j.jpor.2015.02.001
5. Nagata, M. *et al.* A Hedgehog-Foxf axis coordinates dental follicle-derived alveolar bone formation. *Nat Commun* 16, 6061 (2025). https://doi.org/10.1038/s41467-025-61050-3
6. Jing, J. *et al.* Spatiotemporal single-cell regulatory atlas reveals neural crest lineage diversification and cellular function during tooth morphogenesis. *Nat Commun* 13, 4803 (2022). https://doi.org/10.1038/s41467-022-32490-y
7. Takahashi, A. *et al.* Autocrine regulation of mesenchymal progenitor cell fates orchestrates tooth eruption. *Proc Natl Acad Sci U S A* 116, 575–580 (2019). https://doi.org/10.1073/pnas.1810200115
8. Shan, C. *et al.* A spatially organized Cd24a(+)/Pax9(+) stem cell core governs postnatal tooth establishment. *Sci Adv* 11, eadu5653 (2025). https://doi.org/10.1126/sciadv.adu5653
9. Gong, X. *et al.* Tracing PRX1(+) cells during molar formation and periodontal ligament reconstruction. *Int J Oral Sci* 14, 5 (2022). https://doi.org/10.1038/s41368-021-00155-z
10. Xu, X., Gong, X., Zhang, L., Zhang, H. & Sun, Y. PRX1-positive mesenchymal stem cells drive molar morphogenesis. *Int J Oral Sci* 16, 15 (2024). https://doi.org/10.1038/s41368-024-00277-0
11. Feng, J. *et al.* BMP signaling orchestrates a transcriptional network to control the fate of mesenchymal stem cells in mice. *Development* 144, 2560–2569 (2017). https://doi.org/10.1242/dev.150136
12. Xu, C. *et al.* LepR-expressing cells are a critical population in periodontal healing post periodontitis. *J Bone Miner Res* 39, 59–72 (2024). https://doi.org/10.1093/jbmr/zjad008
13. Zhang, D. *et al.* Lepr-Expressing PDLSCs Contribute to Periodontal Homeostasis and Respond to Mechanical Force by Piezo1. *Adv Sci (Weinh)* 10, e2303291 (2023). https://doi.org/10.1002/advs.202303291
14. Palmer, K. *et al.* Discovery and characterization of spontaneous mouse models of craniofacial dysmorphology. *Dev Biol* 415, 216–227 (2016). https://doi.org/10.1016/j.ydbio.2015.07.023

15. Lan, R., Wu, Y., Dai, Q. & Wang, F. Gene mutations and chromosomal abnormalities in syndromes with tooth agenesis. *Oral Dis* 29, 2401–2408 (2023). https://doi.org/10.1111/odi.14402
16. Mostowska, A. *et al.* GREM2 nucleotide variants and the risk of tooth agenesis. *Oral Dis* 24, 591–599 (2018). https://doi.org/10.1111/odi.12793
17. Kantaputra, P. N. *et al.* GREMLIN 2 Mutations and Dental Anomalies. *J Dent Res* 94, 1646–1652 (2015). https://doi.org/10.1177/0022034515608168
18. Vogel, P. *et al.* Malformation of incisor teeth in Grem2$^{-/-}$ mice. *Vet Pathol* 52, 224–229 (2015). https://doi.org/10.1177/0300985814528218
19. Plikus, M. V. *et al.* Cyclic dermal BMP signalling regulates stem cell activation during hair regeneration. *Nature* 451, 340–344 (2008). https://doi.org/10.1038/nature06457
20. Kosinski, C. *et al.* Gene expression patterns of human colon tops and basal crypts and BMP antagonists as intestinal stem cell niche factors. *Proc Natl Acad Sci U S A* 104, 15418–15423 (2007). https://doi.org/10.1073/pnas.0707210104
21. Reddi, A. H. Role of morphogenetic proteins in skeletal tissue engineering and regeneration. *Nat Biotechnol* 16, 247–252 (1998). https://doi.org/10.1038/nbt0398-247
22. McCarthy, N. *et al.* Distinct Mesenchymal Cell Populations Generate the Essential Intestinal BMP Signaling Gradient. *Cell Stem Cell* 26, 391–402.e395 (2020). https://doi.org/10.1016/j.stem.2020.01.008
23. Kraiczy, J. *et al.* Graded BMP signaling within intestinal crypt architecture directs self-organization of the Wnt-secreting stem cell niche. *Cell Stem Cell* 30, 433–449.e438 (2023). https://doi.org/10.1016/j.stem.2023.03.004
24. Worthley, D. L. *et al.* Gremlin 1 identifies a skeletal stem cell with bone, cartilage, and reticular stromal potential. *Cell* 160, 269–284 (2015). https://doi.org/10.1016/j.cell.2014.11.042
25. Krivanek, J. *et al.* Dental cell type atlas reveals stem and differentiated cell types in mouse and human teeth. *Nat Commun* 11, 4816 (2020). https://doi.org/10.1038/s41467-020-18512-7
26. Zhao, H. *et al.* Secretion of Shh by a Neurovascular Bundle Niche Supports Mesenchymal Stem Cell Homeostasis in the Adult Mouse Incisor. *Cell Stem Cell* 23, 147 (2018). https://doi.org/10.1016/j.stem.2018.05.023
27. Men, Y. *et al.* Gli1 + Periodontium Stem Cells Are Regulated by Osteocytes and Occlusal Force. *Dev Cell* 54, 639–654.e636 (2020). https://doi.org/10.1016/j.devcel.2020.06.006
28. Seidel, K. *et al.* Resolving stem and progenitor cells in the adult mouse incisor through gene co-expression analysis. *Elife* 6 (2017). https://doi.org/10.7554/eLife.24712
29. Nigmatullina, L. *et al.* Id2 controls specification of Lgr5(+) intestinal stem cell progenitors during gut development. *Embo j* 36, 869–885 (2017). https://doi.org/10.15252/embj.201694959
30. Jing, J. *et al.* Reciprocal interaction between mesenchymal stem cells and transit amplifying cells regulates tissue homeostasis. *Elife* 10 (2021). https://doi.org/10.7554/eLife.59459

31. Bi, R. *et al.* Function of Dental Follicle Progenitor/Stem Cells and Their Potential in Regenerative Medicine: From Mechanisms to Applications. *Biomolecules* 11 (2021). https://doi.org/10.3390/biom11070997
32. Nagata, M., Ono, N. & Ono, W. Mesenchymal Progenitor Regulation of Tooth Eruption: A View from PTHrP. *J Dent Res* 99, 133–142 (2020). https://doi.org/10.1177/0022034519882692
33. Komori, T. *et al.* Wnt-dependent ontogeny of acellular cementum-forming cementoblasts on the tooth root surface. *Nat Commun* (2026). https://doi.org/10.1038/s41467-026-72712-1
34. Hao, Y. *et al.* Dictionary learning for integrative, multimodal and scalable single-cell analysis. *Nat Biotechnol* 42, 293–304 (2024). https://doi.org/10.1038/s41587-023-01767-y
35. Sharpe, P. T. Dental mesenchymal stem cells. *Development* 143, 2273–2280 (2016). https://doi.org/10.1242/dev.134189
36. Zhou, T. *et al.* Dental Follicle Cells: Roles in Development and Beyond. *Stem Cells Int* 2019, 9159605 (2019). https://doi.org/10.1155/2019/9159605
37. Wang, C. L. *et al.* Gremlin2 Suppression Increases the BMP-2-Induced Osteogenesis of Human Bone Marrow-Derived Mesenchymal Stem Cells Via the BMP-2/Smad/Runx2 Signaling Pathway. *J Cell Biochem* 118, 286–297 (2017). https://doi.org/10.1002/jcb.25635
38. Nolan, K. *et al.* Structure of Gremlin-2 in Complex with GDF5 Gives Insight into DAN-Family-Mediated BMP Antagonism. *Cell Rep* 16, 2077–2086 (2016). https://doi.org/10.1016/j.celrep.2016.07.046
39. Rydze, R. T. *et al.* Deletion of Gremlin-2 alters estrous cyclicity and disrupts female fertility in mice†. *Biol Reprod* 105, 1205–1220 (2021). https://doi.org/10.1093/biolre/ioab148
40. Koffi, K. A. *et al.* The Role of GH/IGF Axis in Dento-Alveolar Complex from Development to Aging and Therapeutics: A Narrative Review. *Cells* 10 (2021). https://doi.org/10.3390/cells10051181
41. Wang, T. *et al.* Skeletal stem/progenitor cell-derived rather than osteoblast-derived IGF2 supports the development and homeostasis of skeletal system via STAT3. *Int J Biol Sci* 21, 3229–3246 (2025). https://doi.org/10.7150/ijbs.112605
42. Deng, Y. *et al.* Gli1(+) Periodontal Mesenchymal Stem Cells in Periodontitis. *J Dent Res* 103, 279–288 (2024). https://doi.org/10.1177/00220345231220915
43. Nolan, K. *et al.* Structure of protein related to Dan and Cerberus: insights into the mechanism of bone morphogenetic protein antagonism. *Structure* 21, 1417–1429 (2013). https://doi.org/10.1016/j.str.2013.06.005
44. Müller, II *et al.* Functional modeling in zebrafish demonstrates that the atrial-fibrillation-associated gene GREM2 regulates cardiac laterality, cardiomyocyte differentiation and atrial rhythm. *Dis Model Mech* 6, 332–341 (2013). https://doi.org/10.1242/dmm.010488
45. Dong, J. *et al.* Elucidation of a universal size-control mechanism in Drosophila and mammals. *Cell* 130, 1120–1133 (2007). https://doi.org/10.1016/j.cell.2007.07.019
46. Wang, X. *et al.* Positional BMP signaling orchestrates villus length in the small intestine. *Nat Commun* 16, 5461 (2025). https://doi.org/10.1038/s41467-025-60643-2

47. Nilsson, K. H. *et al.* GREM2 inactivation increases trabecular bone mass in mice. *Sci Rep* 14, 12967 (2024). https://doi.org/10.1038/s41598-024-63439-4
48. Pei, F. *et al.* FGF signaling modulates mechanotransduction/WNT signaling in progenitors during tooth root development. *Bone Res* 12, 37 (2024). https://doi.org/10.1038/s41413-024-00345-5
49. Zhou, T. *et al.* Gli2 and Gli3 synergistically mediate HH-TGF-β crosstalk in mesenchymal progenitor cells to orchestrate tooth root morphogenesis. *Int J Oral Sci* 18 (2026). https://doi.org/10.1038/s41368-026-00427-6
50. Sun, K. *et al.* A Wnt10a-Notch signaling axis controls Hertwig's epithelial root sheath cell behaviors during root furcation patterning. *Int J Oral Sci* 16, 25 (2024). https://doi.org/10.1038/s41368-024-00288-x

Figures

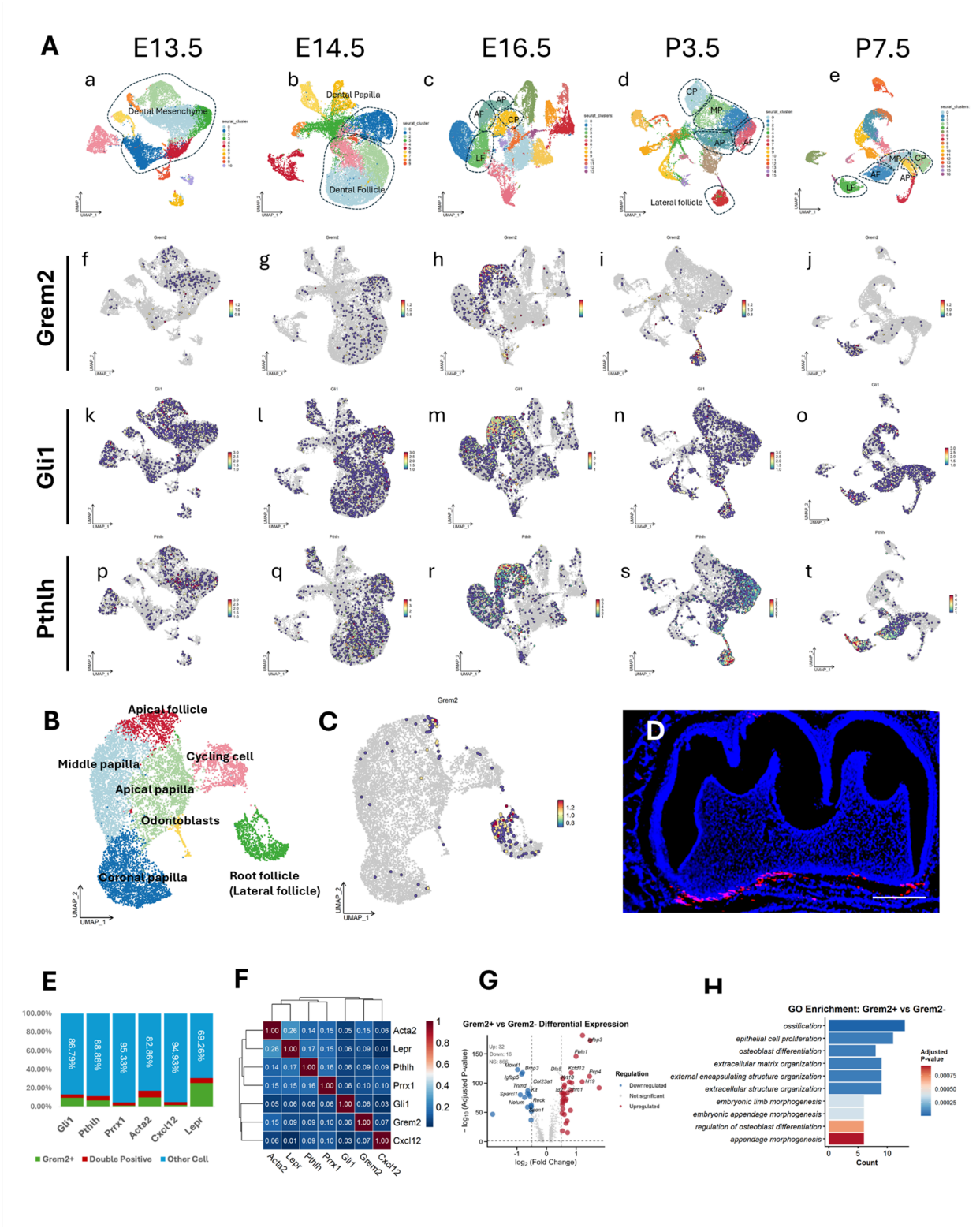


Figure 1

Grem2 marks a distinct dental follicle subpopulation during tooth root development

(A). UMAP visualization showing the distribution of *Grem2*, the dental stem cell marker *Gli1*, and the dental follicle stem cell marker *Pthlh* in integrated molar germs across five developmental stages. **(a–e)** Unsupervised clustering of scRNA-seq data visualized by UMAP. Clusters were annotated according to

previously established criteria. AP, apical pulp; CP, coronal pulp; MP, middle pulp; AF, apical follicle; LF, lateral follicle. Note that the lateral follicle population begins to segregate from other populations starting at P3.5 on UMAP. (f-g) distribution of Grem2 on UMAP; (K-o) distribution of Gli1 on UMAP. (p-t) distribution of Pthlh on UMAP

(B) Re-cluster of mesenchymal populations of P3.5. clusters were annotated according to previous established criteria. Lateral follicle was renamed as root follicle to better fit the distribution and expression of Grem2

(C) Grem2 distributed at a subset of root follicle population.

(D) RNAscope revealed Grem2 gene expression at the dental follicle beneath crown at PN3.5. Scale bar: 200 um.

(E) Stacking histogram of Grem2+ cells and other dental stem cell clusters.

(F) Heatmap depicting the Pearson correlation coefficients of Grem2expression with known dental mesenchymal stem cell markers, including Gli1, Pthlh, Prrx1, Acta2, Cxcl12, and Lepr. Color intensity represents the strength of correlation.

(G) Volcano plot showing DEGs between $Grem2^{+}$ and $Grem2^{-}$ cells. Red dots indicate significantly upregulated genes ($|\log_2 FC| > 1$, adjusted $P < 0.05$); blue dots indicate significantly downregulated genes. Selected genes of interest are labeled.

(H) GO enrichment analysis of differentially expressed genes between $Grem2^{+}$ and $Grem2^{-}$ cells. The bar plot shows the top enriched biological process terms ranked by significance.

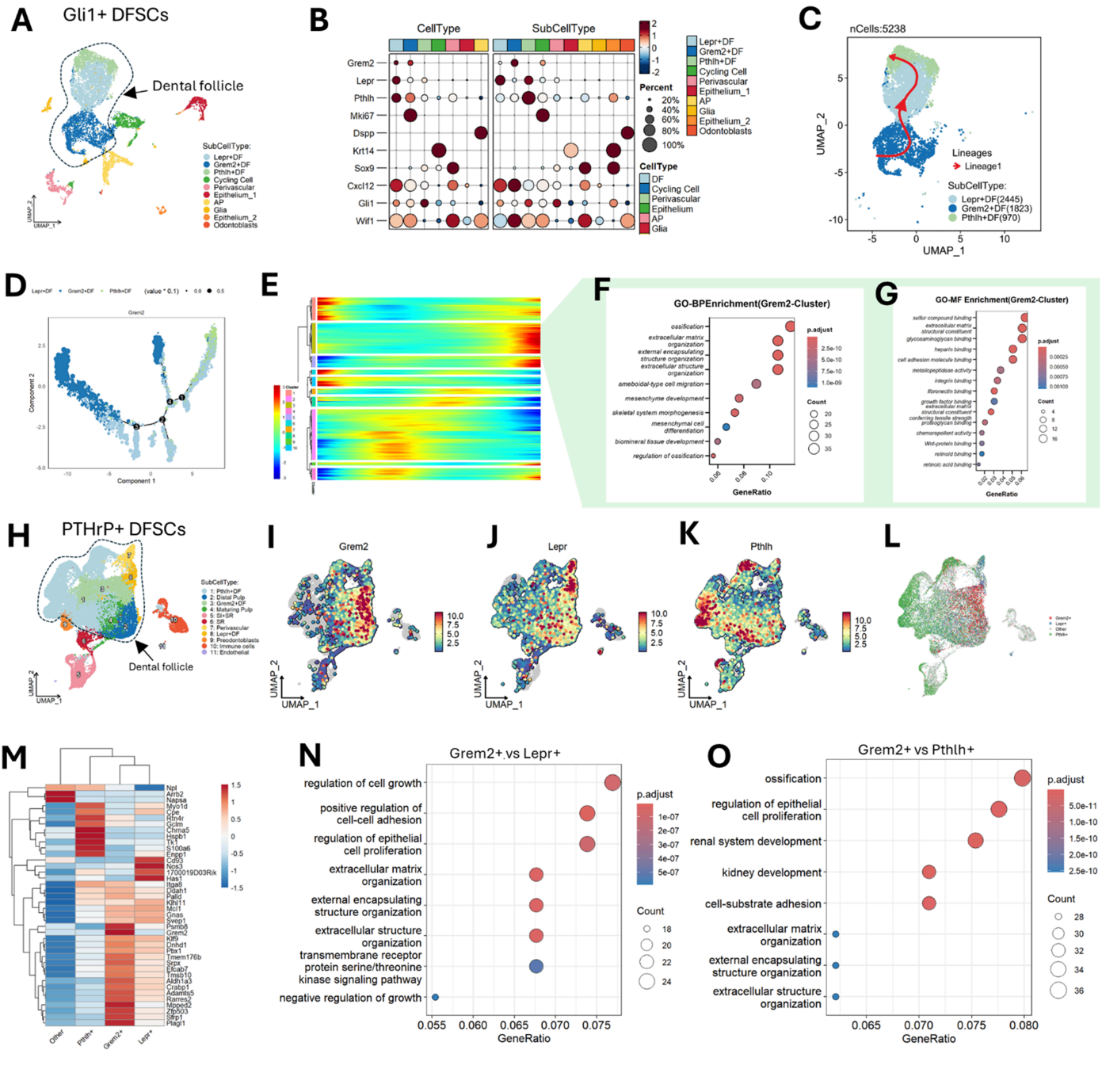


Figure 2

Grem2⁺ Cells Represent a Distinct Progenitor Population of the Dental Follicle

(A) scRNA-seq analysis of Gli1-GFP⁺ cells isolated by FACS from the molars of *Gli1*$^{GFP/+}$;*Pthrp-creER*;*R26R*^{tdTomato}mice, traced from PN3 to PN6(GSE237439).

(B) Dot plot showing the expression levels (color intensity) and the percentage of expressing cells (dot size) for selected genes across major cell types (CellType) and their corresponding subtypes

(SubCellType) in the dental mesenchyme. Notably, the dental follicle population is heterogeneous, and none of Grem2, Lepr, Pthlh, Cxcl12, or Gli1alone could specifically mark the entire dental follicle cell type. Instead, subclustering the dental follicle population into Grem2$^+$, Lepr$^+$, and Pthlh$^+$ subtypes provided better annotation of each cluster.

(C) Slingshot differentiation trajectory of dental follicle population.

(D) Monocle2 differentiation trajectory of dental follicle population.

(E) Unsupervised clustering of genes along the Monocle 2 differentiation trajectory.

(F) GO Biological Process (BP) enrichment analysis of genes co-clustered with Grem2 based on pseudotime trajectory inference.

(G) GO Molecular Function (MF) enrichment analysis of genes co-clustered with Grem2 based on pseudotime trajectory inference.

(H) scRNA-seq analysis of PTHrP-mCherry$^+$ cells FACS-sorted from mandibular tissues at P6, P15, P25, and 8 weeks (GSE313714 and GSE120108). Clusters were annotated according to previous criteria and the expression of Grem2, Lepr, and Pthlh.

(I) The distribution of *Grem2* on UMAP of PTHrP+ DFSCs.

(J) The distribution of *Lepr* on UMAP of PTHrP+ DFSCs.

(K) The distribution of *Pthlh* on UMAP of PTHrP+ DFSCs.

(L) UMAP visualization showing the expression distribution of Grem2, Lepr, and Pthlhin the dental mesenchyme. These three genes label adjacent but distinct cellular subpopulations within the dental follicle.

(M) Heatmap showing differential gene expression across Grem2$^+$, Lepr$^+$, Pthlh$^+$ subpopulations. Expression values are z-score normalized; red and blue indicate upregulated and downregulated genes, respectively.

(N) GO enrichment analysis of DEGs between Grem2$^+$ and Lepr$^+$ dental follicle subpopulations.

(O) GO enrichment analysis of DEGs between Grem2$^+$ and Pthlh$^+$ dental follicle subpopulations.

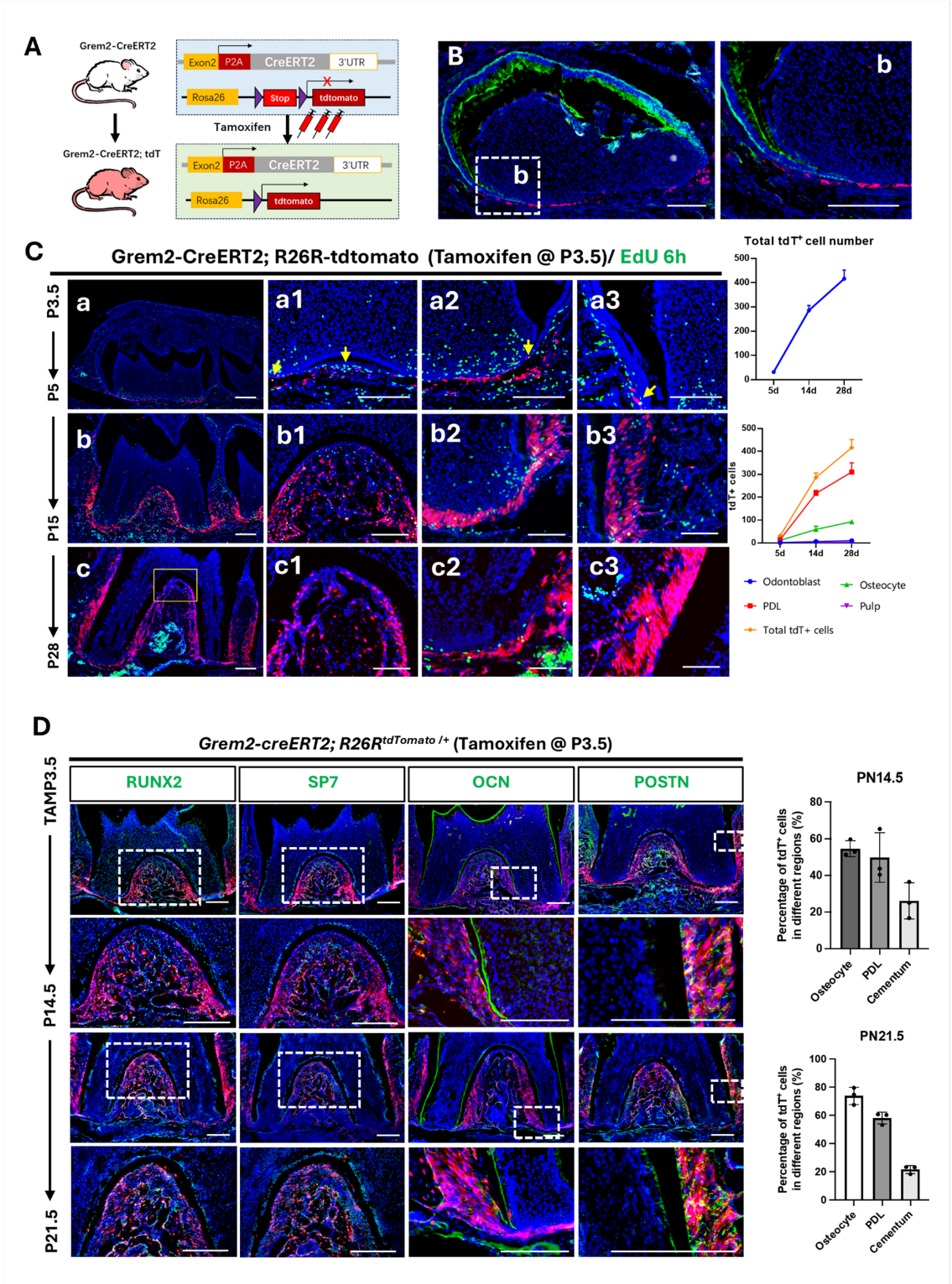


Figure 3

Grem2⁺ Cells Contribute to Interradicular Alveolar Bone, Periodontal Ligaments, and Cementoblasts

(A). Experimental design schematic for lineage tracing using *Grem2-CreERT2.* A targeting strategy was designed to replace the endogenous stop codon in exon 2 of the Grem2gene with a “P2A-CreERT2” cassette via CRISPR/Cas9-mediated homologous recombination. The 3' untranslated region (3' UTR) is

retained downstream of the cassette to preserve endogenous mRNA stability and regulation. Upon tamoxifen administration, CreERT2 translocates to the nucleus, excises the loxP-flanked stop cassette in the Rosa26-tdTomatoreporter allele, and permanently labels Grem2$^+$ cells and their progeny with tdTomato fluorescence.

(B) Pulse-chase tracing of Grem2$^+$ cells from PN1.5 to PN3.5. Epithelium was labeled by Krt14 immunofluorescence. **(b)** Grem2$^+$ cells were localized to the dental follicle beneath the epithelium, with no overlap between Grem2$^+$ cells and epithelial cells. Scale bar: 200 um in Figure B, and 100 um in Figure B,b

(C). Lineage tracing of Grem2$^+$ cells from PN3.5. EdU was administrated 6 hours before sacrifice. **(a–c)** Grem2$^+$ cells and their derivatives traced from PN3.5 to PN5.5 (a), PN14 (b), and PN28 (c). **(a1–c1)** Higher magnification views of the root furcation area. **(a2–c2)** Higher magnification views of the root elongation front, corresponding to the terminal end of the double-layered enamel epithelium of Hertwig's epithelial root sheath (HERS). **(a3–c3)** Higher magnification views of the periodontal ligament (PDL). Scale bar: 200 um in (a-c), and 100 um in (a1-c3);

(D). Dental marker analysis of lineage-traced Grem2+ cells. lineage tracing was performed with Tamoxifen induction at PN3.5. Tissues were harvested at PN21. Red, tdtomato+ cells (Grem2 tracing); green, dental markers, including Runx2 and Sp7 (osteogenic activity), OCN (cemenblasts), and Postn (PDLs). Scale bar: 200 um

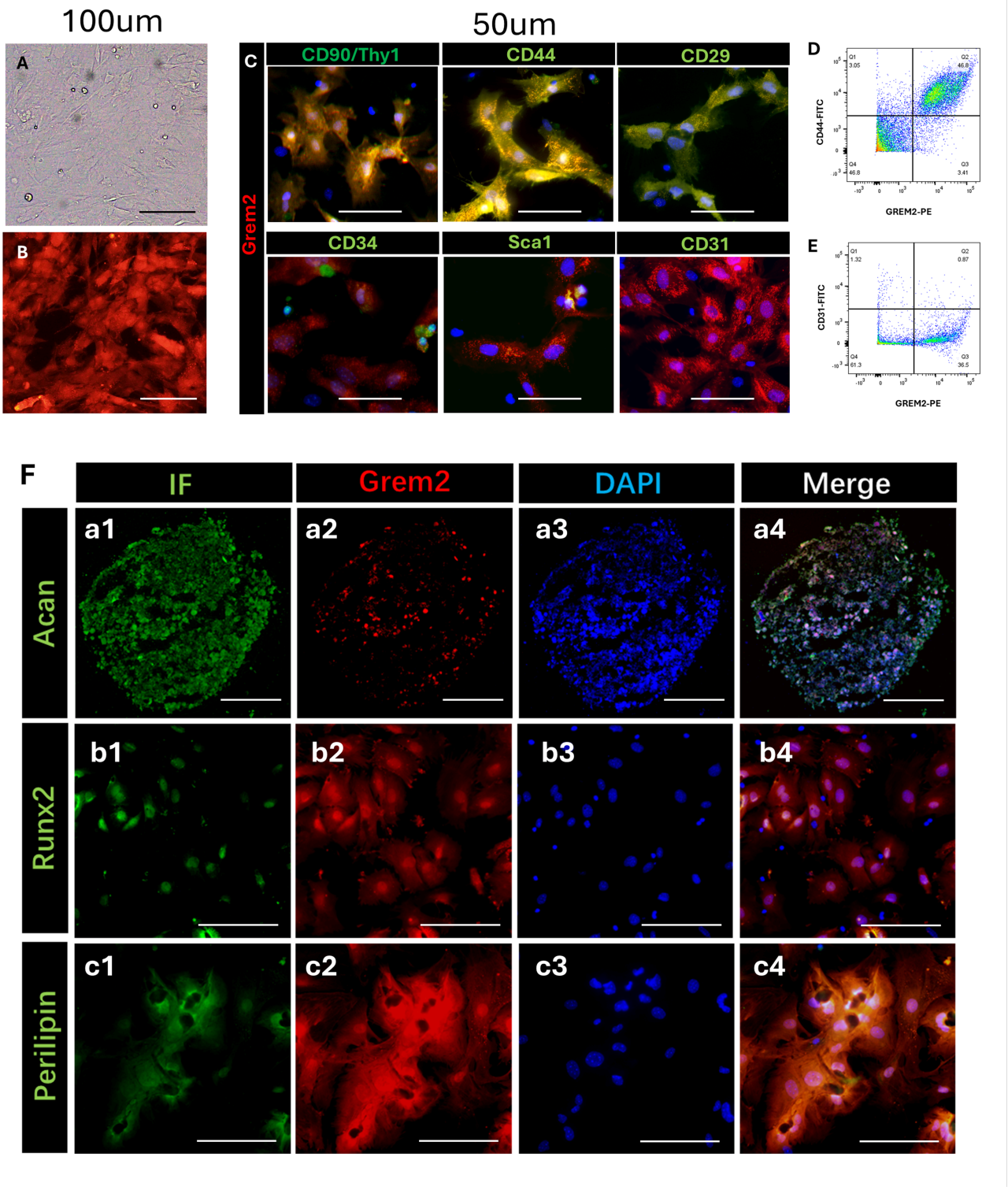


Figure 4

Grem2⁺ Cells Exhibit Mesenchymal Stem Cell Properties In Vitro

(A) Bright-field microscopy image of in vitro cultured dental pulp stem cells (DPSCs) at passage 3. Cells were isolated from PN5 *Grem2-CreERT2; tdTomato*mice; tamoxifen was administered at PN3.5. Scale bar: 100 um

(B) Fluorescence microscopy image of in vitro cultured DPSCs. Red fluorescence indicates Grem2^{+} cells. Scale bar: 100 um

(C) Colocalization of Grem2^{+} cells with the mesenchymal stem cell marker CD90/Thy1, CD44, CD29. And absence of colocalization between Grem2^{+} cells and the mesenchymal stem cell negative marker CD34, Sca1, CD31. Scale bar: 50 um

(D) Flow cytometry analysis of DPSCs from *Grem2-CreERT2; tdTomato*mice; cells were stained for CD44.

(E) Flow cytometry analysis of DPSCs from *Grem2-CreERT2; tdTomato*mice; cells were stained for CD31.

(F) Trilineage differentiation of DPSCs from *Grem2-CreERT2; tdTomato*mice. **(a1–a4)** Chondrogenic differentiation; **(b1–b4)** Osteogenic differentiation; **(c1–c4)** Adipogenic differentiation. Scale bar: 100 um

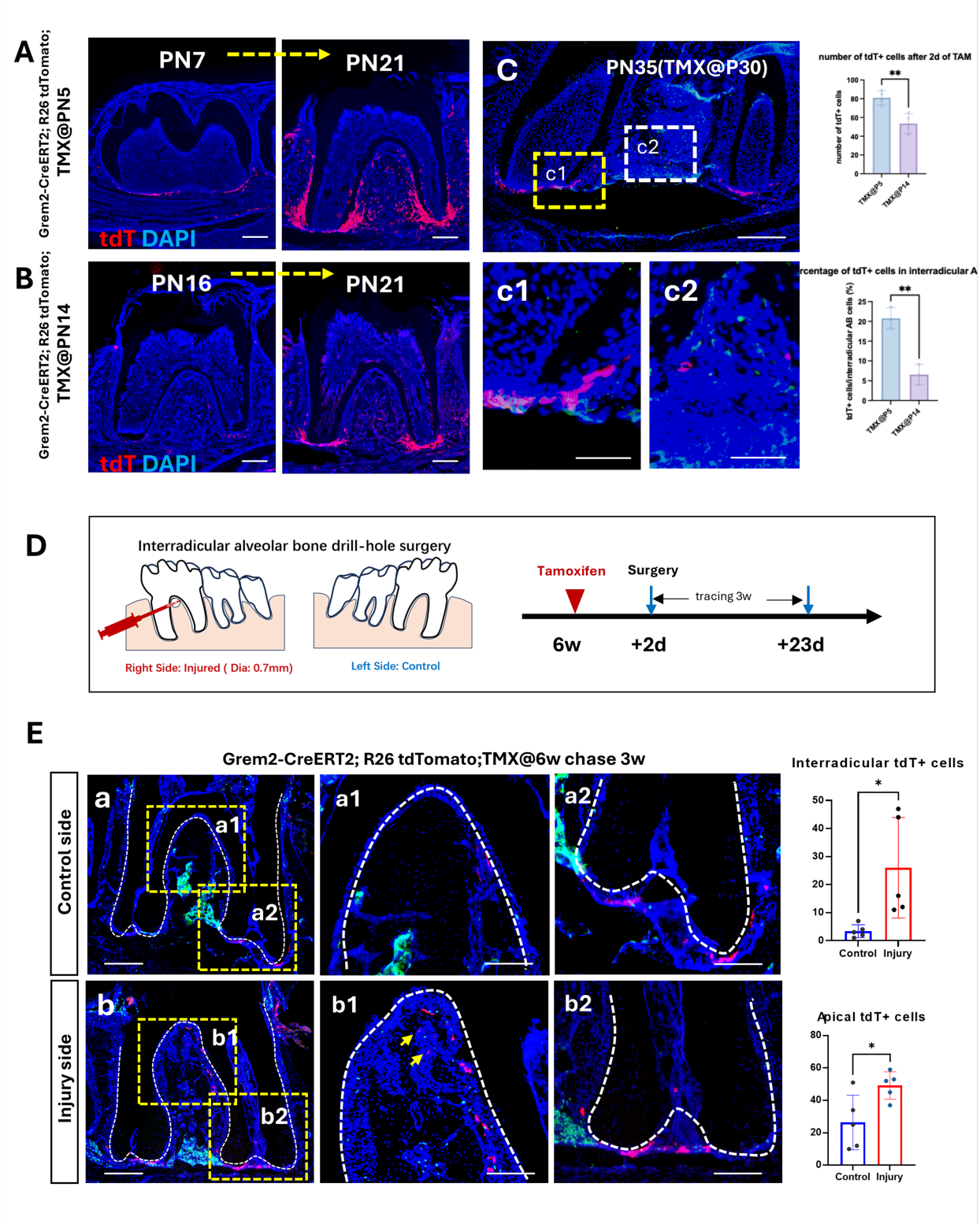


Figure 5

Grem2⁺ Cells Continuously Contribute to Periodontal Tissue Development, Persist into Adulthood, and Respond to Tissue Regeneration

(A) Lineage tracing of Grem2⁺ cells from PN5 to PN7 and PN21. Scale bar: 200 um

(B) Lineage tracing of Grem2$^+$ cells from PN14 to PN16 and PN21. Scale bar: 200 um

(C) Lineage tracing of Grem2$^+$ cells from PN30 to PN35. **(c1)** Higher magnification view of Grem2$^+$ cells at the root elongation front. **(c2)** Higher magnification view of Grem2$^+$ cells in the interradicular alveolar bone. Scale bar: 200 um in (A-C), and 100 um in (c1-c2)

(D) Experimental design schematic for the interradicular alveolar bone injury assay. Six-week-old *Grem2-CreERT2; R26-tdTomato*mice were administered tamoxifen. The interradicular alveolar bone on the right side was injured using a 22G (0.7 mm × 25 mm) hypodermic needle 2 days post tamoxifen administration. The contralateral left side served as the untreated control. Mice were traced for 21 days post-injury. EdU was administered 6 hours prior to sacrifice.

(E) Lineage tracing of Grem2$^+$ cells following interradicular alveolar bone injury. **(a)** Control side. **(a1)** Higher magnification view of the interradicular alveolar bone area. **(a2)** Higher magnification view of the root apical area. **(b)** Injured side. **(b1)** Higher magnification view of the interradicular alveolar bone area. **(b2)** Higher magnification view of the root apical area. Scale bar: 200 um in (E), and 100 um in (a1-b2)

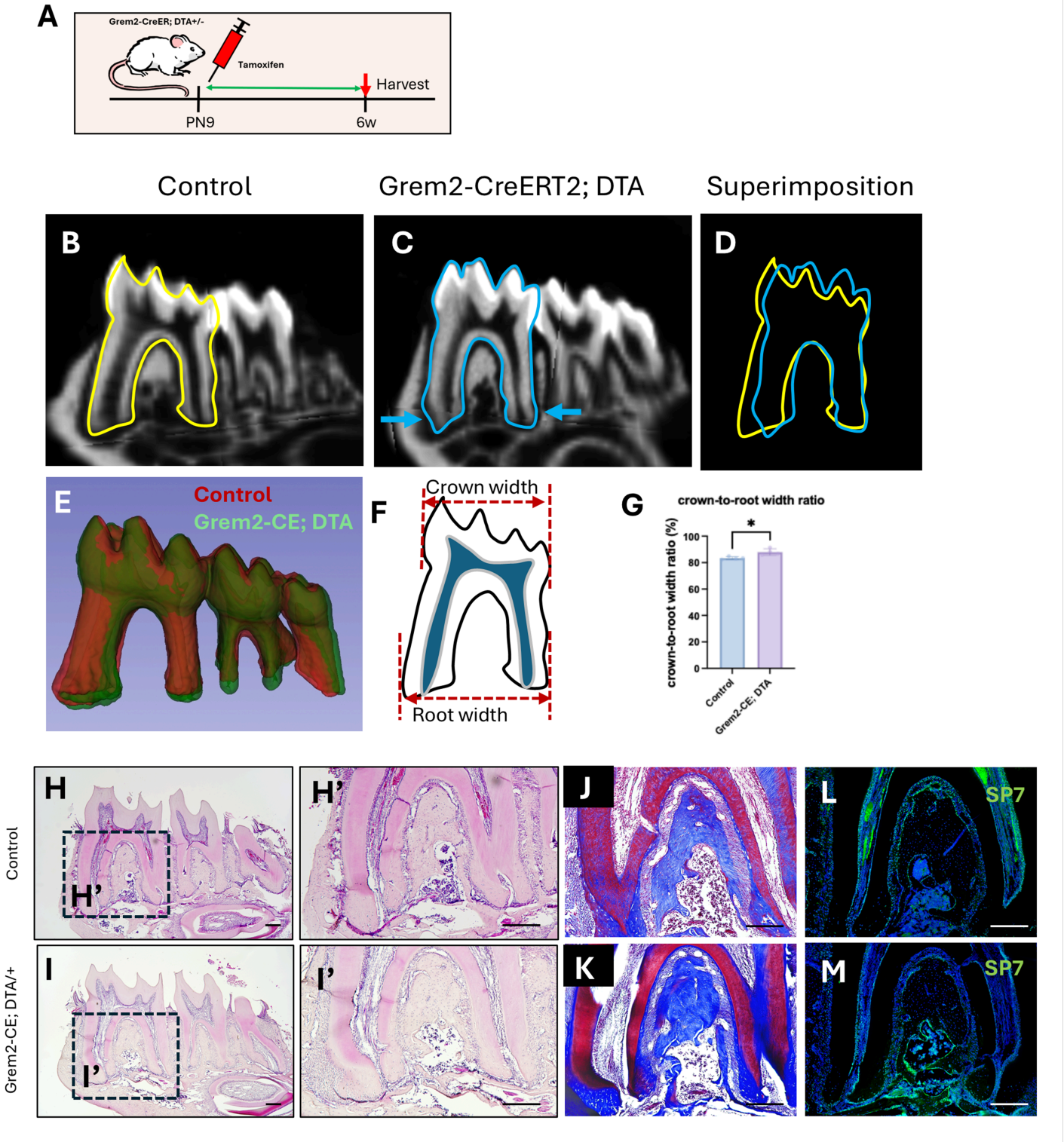


Figure 6

Ablation of Grem2⁺ Cells Impairs Interradicular Alveolar Bone Formation

(A) Experimental design schematic for Grem2⁺ cell ablation. *Grem2-CreERT2*mice were crossbred with *R26-DTA*mice. Tamoxifen was administered at PN9, and samples were harvested at 6 weeks.

(B-F) Micro-CT analysis of molars between Control (DTA/+) mice and Grem2-CreERT2; DTA/+ mice at 6 weeks. (B) sagittal section of mandible first molar of Control (DTA/+) mice. The contour of mandible first molar was outlined with yellow line. (C) sagittal section of mandible first molar of Grem2+ cell ablation (Grem2-CreERT2; DTA/+) mice. The contour of mandible first molar was outlined with blue line. (D) superimposition of the contour of the mandibular first molar between Control mice and Grem2-CreERT2; DTA/+ mice. reference was set at the root furcation and distal root. (E) three-dimensional superimposition of the contour of the mandibular molars between Control mice and Grem2-CreERT2; DTA/+ mice. reference was set at the root furcation and distal root. (F) the maximal crown width as well as the root width (the distance between the mesial and distal root) was illustrated. (G) Increased crown to root width ratio in Grem2-CreERT2; DTA/+ mice compared to control mice. n=4 ,* $P<0.05$

(H) H&E staining of molars of Control mice (Grem2-CreERT2). H': Higher magnification view of control mice at the interradicular alveolar bone

(I) H&E staining showed narrowed root width between mesial and distal root of Grem2-CreERT2; DTA/+ mice. I': Higher magnification view of Grem2-CreERT2; DTA/- mice at the interradicular alveolar bone

(J) Masson staining of molars of Control mice (Grem2-CreERT2) at the interradicular alveolar bone region

(K) Masson staining of molars of Grem2-CreERT2; DTA/+ mice showed increased bone density at the cervical portion of the interradicular bone.

(L) Sp7 immunostaining showed active osteogenic activity at the cervical portion of the interradicular bone of Control mice.

(M) Sp7 immunostaining showed decreased osteogenic activity at the cervical portion of the interradicular bone in Grem2-CreERT2; DTA/+ mice.

Scale bar: 200 um

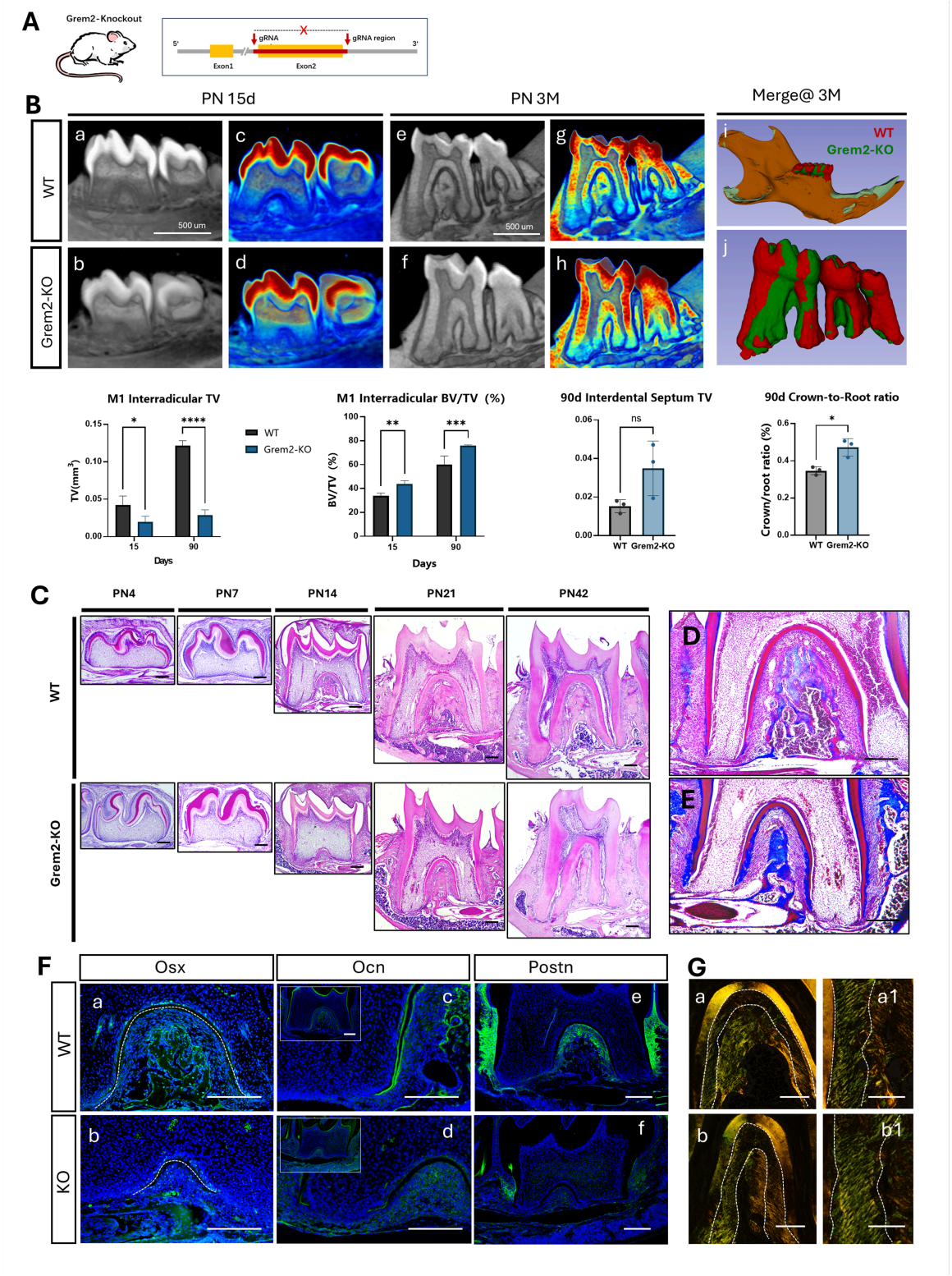


Figure 7

Grem2 Deficiency Impairs Interradicular Alveolar Bone Formation

(A) Schematic of the CRISPR-Cas9 strategy used to generate *Grem2*-KO mice. Exon 2 of the *Grem2*gene was deleted via dual sgRNA-guided Cas9 cleavage, resulting in a null allele.

(B) Micro-CT comparison between WT and *Grem2*-KO mice. **(a–h)** Sagittal sections of the mandibular first molar traversing both mesial and distal roots. **(a,b,e,f)** Sections in black-and-white rendering. **(c,d,g,h)** Sections in pseudo-color, where red indicates high mineralization density and blue indicates low mineralization density. **(i)** Three-dimensional reconstruction of WT and *Grem2*-KO mandibles, overlaid using the mandibular border as a reference. **(j)** Overlay of the mandibular first molars of WT (red) and *Grem2*-KO (green) using the crown as a reference.

(C) Time-series sections of mandibular first molars from WT and *Grem2*-KO mice from PN4 to PN42. Scale bar: 200 um

(D) Masson staining of mandibular first molar sections from WT mice.

(E) Masson staining of mandibular first molar sections from *Grem2*-KO mice.

(F) Immunofluorescent staining for Osx (osteogenic differentiation), Ocn (cementum differentiation), and Postn (PDL differentiation) at PN14, revealing compromised generation of alveolar bone, cementum, and PDL fibroblasts in Grem2-KO mice.

(G) Sirius red staining of WT (a) and *Grem2*-KO (b) mice. **(a1,b1)** Magnified views of the periodontal ligament (PDL).

Scale bar: 200 um in (C-F), 100 um in (G, a-b), 50 um in (G, a1-b1)

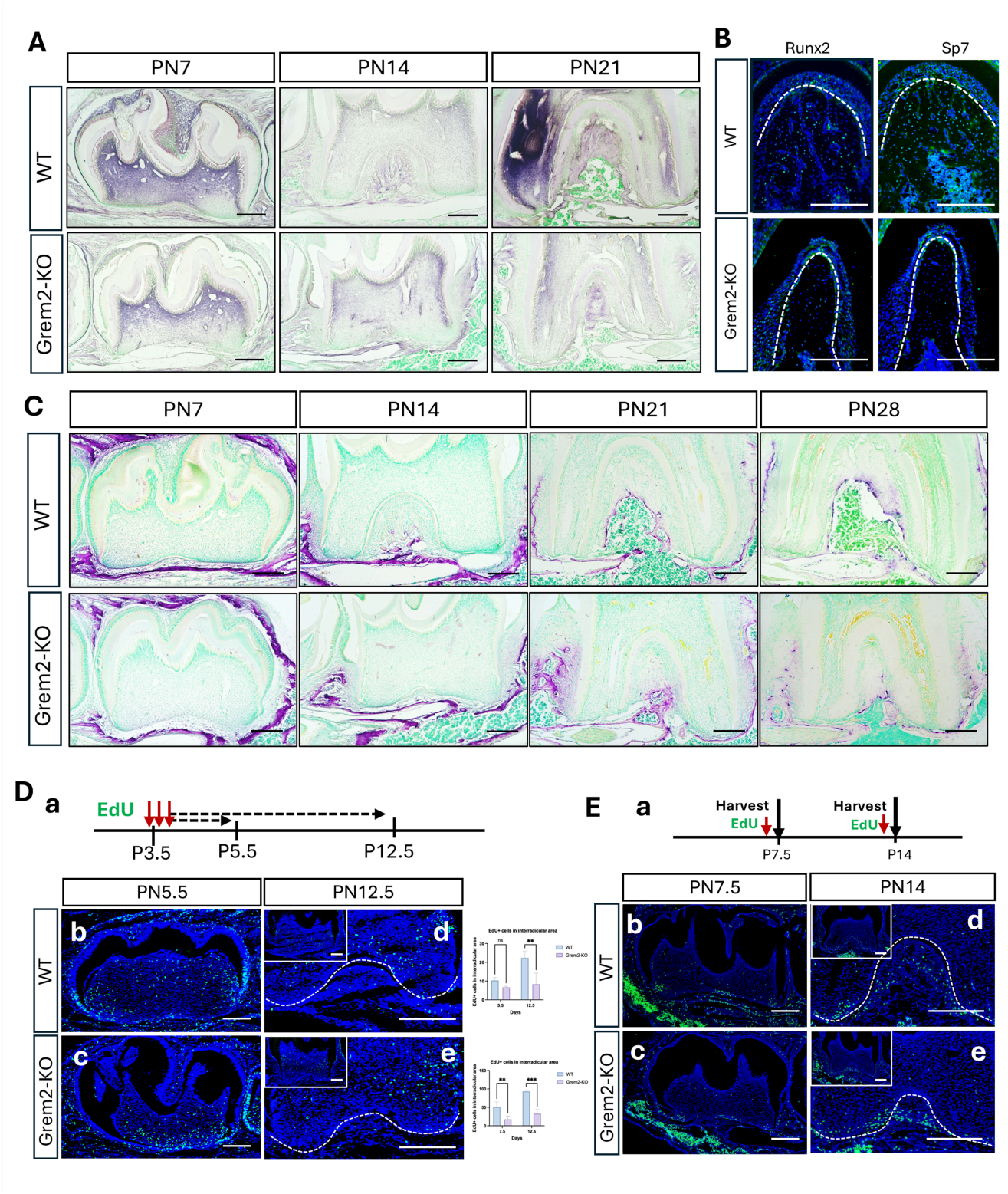


Figure 8

Grem2 knockout impairs interradicular alveolar bone turnover

(A) Serial ALP staining revealed decreased osteogenic activity at the interradicular bone of *Grem2*-KO mice. Scale bar: 200 μm.

(B) Immunofluorescence staining of RUNX2 and SP7 confirmed reduced osteogenic activity in the interradicular alveolar bone of *Grem2*-KO mice. Scale bar: 200 μm.

(C) Serial TRAP staining showed diminished osteoclastic activity at the interradicular bone of *Grem2*-KO mice. Scale bar: 200 μm.

(D) EdU retention assay comparing WT and *Grem2*-KO mice. (a) Experimental strategy: EdU was administered at PN3.5 for three doses, and samples were collected at PN5.5 or PN12.5. (b–e) At both time points, EdU-retaining cells were reduced in the root follicle and interradicular region of *Grem2*-KO mice. n = 3; Scale bar: 200 μm.

(E) Proliferation assay comparing WT and *Grem2*-KO mice. (a) Experimental strategy: a single dose of EdU was injected 6 hours prior to sacrifice at PN7.5 or PN15. (b–e) At both stages, proliferating cells were decreased in the root follicle and interradicular area of *Grem2*-KO mice. n = 3; Scale bar: 200 μm.

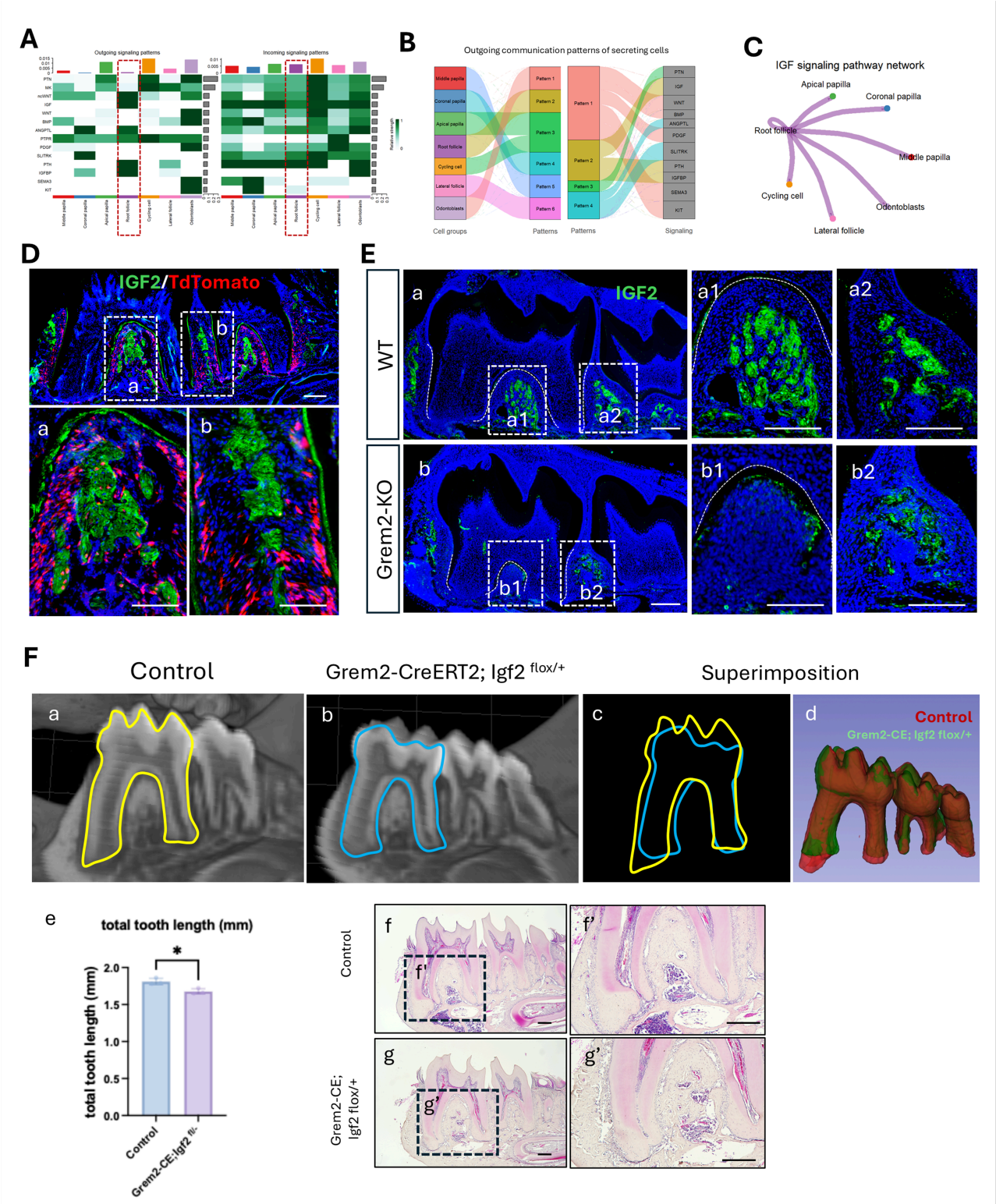


Figure 9

Grem2⁺ DFSCs Communicate with Other Cell Populations Through IGF Signaling

(A) Heatmap of outgoing and incoming signaling interactions among cell cluster populations. Note that ncWNT, IGF, PTH, and IGFBP signaling were enriched in the outgoing signals of the root follicle cluster, whereas PTH signaling was enriched in its incoming signals.

(B) Sankey diagram of cell outgoing communication patterns. The root follicle cluster exhibits a unique signaling pattern characterized by IGF, PTH, and IGFBP signaling.

(C) IGF signaling pathway network between cell clusters.

(D) Immunofluorescence staining of IGF2 showing colocalization with Grem2^{+}-derived cells. Grem2^{+}-derived cells were traced from PN3.5 to PN21. **(a)**
Magnified view of the interradicular alveolar bone. **(b)**
Magnified view of the interseptal alveolar bone between the mandibular first and second molars. Scale bar: 200 um

(E) Immunofluorescence staining of IGF2 in WT and *Grem2*-KO mice at PN14. **(a1,b1)**
Magnified views of the interradicular alveolar bone. **(a2,b2)**
Magnified views of the interseptal alveolar bone between the mandibular first and second molars. Scale bar: 200 um

(F) Micro-CT comparison between control and *Grem2-CreERT2; Igf2*$^{flox/+}$ mice. (a) sagittal section of mandible first molar of Control Grem2-CreERT2) mice. The contour of mandible first molar was outlined with yellow line. (b) sagittal section of mandible first molar of Grem2+ cell ablation (Grem2-CreERT2; Igf2 flox/+) mice. The contour of mandible first molar was outlined with blue line. (c) superimposition of the contour of the mandibular first molar between Control mice and Grem2-CreERT2; Igf2 flox/+ mice. reference was set at the root furcation and distal root. (d) three-dimensional superimposition of the contour of the mandibular molars between Control mice and Grem2-CreERT2; Igf2 flox/+ mice. reference was set at the root furcation and distal root. (e) total tooth height was reduced in Grem2-CreERT2; Igf2 flox/+ mice compared to control mice. n=3 ,* $P<0.05$ (f) H&E staining of molars of Control mice (Igf2$^{flox/+}$ mice) . f': Higher magnification view of control mice at the interradicular alveolar bone. (g) H&E staining of molars of Grem2-CreERT2; Igf2$^{flox/+}$ mice showed shorter mesial root and decreased cementoblasts. f': Higher magnification view of Grem2-CreERT2; Igf2$^{flox/+}$ mice at the interradicular alveolar bone.

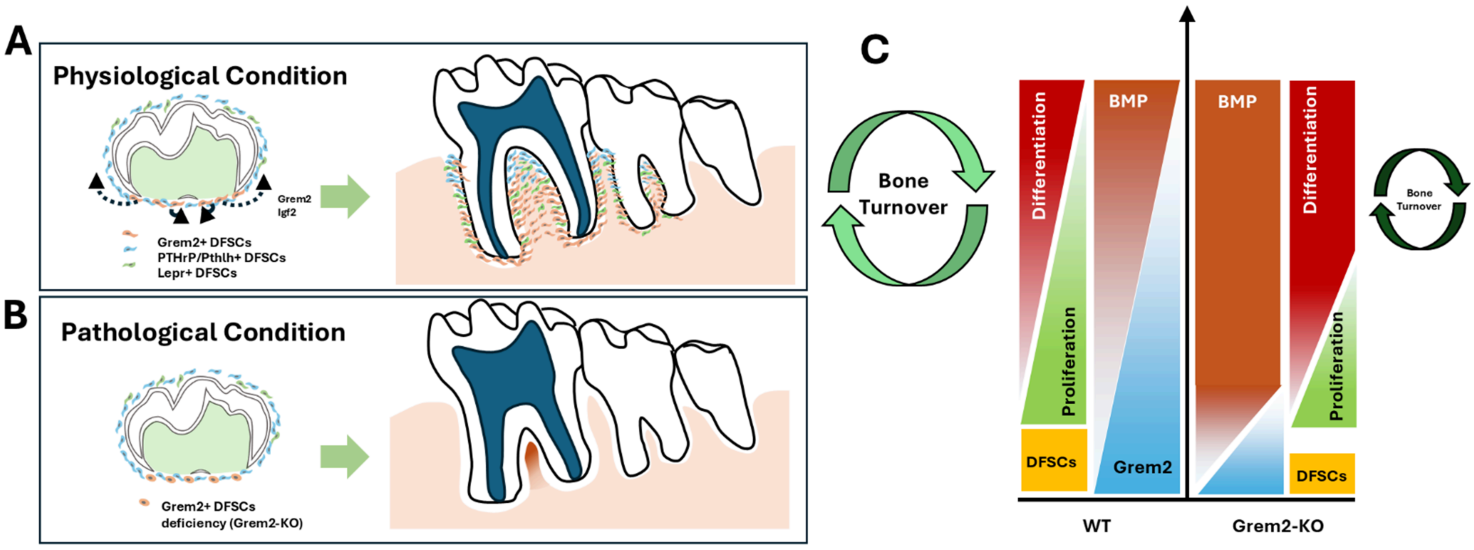


Figure 10

Schematic summary of the role of Grem2⁺ cells in tooth development.

(A) Grem2⁺ DFSCs represent a novel dental follicle stem cell population distinct from PTHrP⁺ and Lepr⁺ cells. These cells contribute to periodontal tissue development, particularly the formation of interradicular alveolar bone. Grem2⁺ cells secrete Grem2 and IGF2 to regulate the local stem cell niche microenvironment.

(B) Grem2 knockout disrupts the root-forming microenvironment, resulting in decreased volume but increased density of interradicular alveolar bone, along with a taurodontism-like phenotype.

(C) Proposed pathological model of Grem2 deficiency-impaired interradicular alveolar bone formation: Grem2-expressing cells secrete Grem2 into the DFSC niche, where it maintains stemness by fine-tuning the balance between proliferation and differentiation. Loss of Grem2 leads to excessive BMP signaling within the niche, causing premature exhaustion of DFSCs and accelerated differentiation of progenitor cells. Consequently, bone turnover declines, manifesting as reduced interradicular alveolar bone remodeling.

Supplementary Files

This is a list of supplementary files associated with this preprint. Click to download.

- SupplementaryFig1.tif